# Terrestrial carbon isotope stratigraphy and mammal turnover during post-PETM hyperthermals in the Bighorn Basin, Wyoming, USA

Sarah J. Widlansky[1], Ross Secord[2], Kathryn E. Snell[3], Amy E. Chew[4], William C. Clyde[1]

[1]Department of Earth Sciences, University of New Hampshire, Durham, NH, 03824, USA
[2]Department of Earth and Atmospheric Sciences, University of Nebraska – Lincoln, Lincoln, NE, 68588, USA
[3]Department of Geological Sciences, University of Colorado Boulder, Boulder, CO, 80309, USA
[4]Department of Ecology and Evolutionary Biology, Brown University, Providence, RI, 02912, USA

*Correspondence to*: Sarah J. Widlansky (sarah.widlansky@unh.edu)

**Abstract.** Paleogene hyperthermals, including the Paleocene-Eocene Thermal Maximum (PETM) and several other smaller events, represent global perturbations to Earth's climate system and are characterized by warmer temperatures, changes in floral and faunal communities, and hydrologic changes. These events are identified in the geologic record globally by negative carbon isotope excursions (CIEs), resulting from the input of isotopically light carbon into Earth's atmosphere. Much about the causes and effects of hyperthermals remains uncertain, including whether all hyperthermals were caused by the same underlying processes, how biotic effects scale with the magnitude of hyperthermals, and why CIEs are larger in paleosol carbonates relative to marine records. Resolving these questions is crucial for a full understanding of the causes of hyperthermals and their application to future climate scenarios. The primary purpose of this study was to identify early Eocene hyperthermals in the Fifteenmile Creek area of the south-central Bighorn Basin, Wyoming U.S.A. This area preserves a sequence of fluvial floodplain sedimentary rocks containing paleosol carbonates and an extensive record of fossil mammals. Previous analysis of faunal assemblages in this area revealed two pulses of mammal turnover and changes in diversity interpreted to correlate with the ETM2 and H2 hyperthermals that immediately follow the PETM. This was, however, based on long distance correlation of the fossil record in this area to chemostratigraphic records from elsewhere in the basin.

We present new carbon isotope stratigraphies using micrite $\delta^{13}C$ values from paleosol carbonate nodules preserved in and between richly fossiliferous localities at Fifteenmile Creek to identify the stratigraphic positions of ETM2 and H2. Carbon isotope results show that the ETM2 and H2 hyperthermals, and possibly the subsequent I1 hyperthermal, are recorded at Fifteenmile Creek. ETM2 and H2 overlap with the two previously recognized pulses of mammal turnover. The CIEs for these hyperthermals are also somewhat smaller in magnitude than in more northerly Bighorn Basin records. We suggest that basin-wide differences in soil moisture and/or vegetation could contribute to variable CIE amplitudes in this and other terrestrial records.

**Deleted:** Carbon isotope stratigraphy and mammal turnove during post-PETM hyperthermals ¶

**Deleted:** sjw2008@wildcats.

**Deleted:** shifts

**Deleted:** are

**Deleted:** their

**Deleted:** interpretation

**Deleted:** The

**Deleted:** central

**Deleted:** , exposes an early Eocene floodplain sedimentary sequence that preserves

**Deleted:** collection

**Deleted:** stratigraphy

**Deleted:** Additionally, we used differential GPS elevations to establish a new stratigraphic framework that assists in correlation and is independent from the biostratigraphy and previous compos lithostratigraphic sections from the area.

**Deleted:** Comparisons between the new chemostratigraphy and fossil record suggest that the recorded amplitude of these faunal changes may be muted as a result of some stratigraphic averaging fossils. …

## 1 Introduction

### 1.1 Paleogene hyperthermals

The early Paleogene is punctuated by numerous short duration (lasting 50–200 kyr) warming events known as "hyperthermals" (Thomas et al., 2000; Westerhold et al., 2018; Barnet et al., 2019). These hyperthermals are characterized by their rapid onset (estimates for some range from less than 10 kyr to ~20 kyr) and are associated with significant negative isotope excursions in $\delta^{13}C$ and $\delta^{18}O$ in marine sedimentary records, and negative $\delta^{13}C$ excursions in terrestrial records, worldwide (e.g., Kennett and Stott, 1991; Koch et al., 1992; Zachos et al., 2001, 2008; Abels et al., 2012, 2016; Westerhold et al., 2020). Many of these hyperthermals are orbitally paced, often occurring during eccentricity maxima in 100 and 405 kyr cycles (Cramer et al., 2003; Lourens et al., 2005; Zachos et al., 2010; Dinarès-Turell et al., 2014; Abels et al., 2016; Barnet et al., 2019; although see D'Onofrio et al., 2016 for debate about which carbon isotope variations during the Paleogene constitute a hyperthermal). The largest and best known of these hyperthermals is the Paleocene–Eocene Thermal Maximum (PETM) at ~56 Ma, during which time global temperatures increased between 5–8° C (McInerney and Wing, 2011). Along with this warming came deep-ocean acidification and carbonate dissolution, and the extinction of 30–50% of benthic foraminifera (Thomas, 1998, 2007; Zachos et al., 2005; Speijer et al., 2012). Conversely, planktic foraminifera experienced geographic range shifts and proliferation over the same interval (Lu and Keller, 1995; Thomas and Shackleton, 1996; Kelly et al., 1998; Gibbs et al., 2006; Agnini et al., 2007; Mutterlose et al., 2007).

The negative carbon isotope excursions (CIEs) associated with the hyperthermals indicate massive injections of isotopically light carbon into the atmosphere, but the source and mechanism of release of these greenhouse gases is unresolved (Higgins and Schrag, 2006). Proposed sources of carbon for the PETM include destabilized methane clathrates (Dickens et al., 1995, 1997; Katz et al., 1999), volcanism associated with the North Atlantic Igneous Province (NAIP) (Gutjahr et al., 2017), thermogenic methane released from organic-rich sediments during NAIP emplacement (Svensen et al., 2004; Frieling et al., 2016), Antarctic permafrost thaw (DeConto et al., 2010, 2012), wildfires burning Paleocene peat deposits (Kurtz et al., 2003; Moore and Kurtz, 2008), and evaporation of epicontinental seas leading to the oxidation of organic matter (Higgins and Schrag, 2006), although geological evidence supporting the last two hypotheses is weak. It is also possible that multiple mechanisms and sources may have acted together and that the drivers may not have been the same for the PETM and smaller hyperthermals. Although the initial trigger for many hyperthermals may be related to orbital cyclicity, the primary cause of warming is likely the associated release of greenhouse gases. Of the smaller hyperthermals, those immediately following the PETM are currently the best studied. These include the Eocene Thermal Maximum 2 (ETM2) at ~54 Ma, also referred to as ELMO (Lourens et al., 2005) or H1 (Cramer et al., 2003), as well as the succeeding H2, I1, and I2 hyperthermals. Like the PETM, these hyperthermals are associated with negative CIEs, increased $CaCO_3$ dissolution, and foraminiferal turnover (Agnini et al., 2009; Stap et al., 2009, 2010; Jennions et al., 2015; Arreguin-Rodriguez and Alegret, 2016; D'Onofrio et al., 2016). The ETM2, H2, and I1 hyperthermals have also been linked to increased radiolarian abundance as well as shifts in calcareous plankton assemblages. Together these suggest upper water column warming, weakening thermal stratification in the upper water column, and

Deleted: ; Thomas et al., 2000

increased nutrients in surface waters during the events (D'Onofrio et al., 2016). The high-resolution marine record of the PETM and subsequent hyperthermals has led to a growing understanding of their effects in the ocean. A similar level of detail has not been developed for the terrestrial record of the smaller (non-PETM) hyperthermals. Achieving this level of understanding will require geochemical records from a variety of depositional environments and locations to fully understand spatial heterogeneity and underlying carbon cycle–climate dynamics. Furthermore, understanding the effects of these hyperthermals on the terrestrial ecosystem requires their recognition in richly fossiliferous strata, where both plant and vertebrate fossils occur in abundance.

### 1.2 Terrestrial record of hyperthermals

Terrestrial stratigraphic records of the PETM have been reported from North America (e.g., Koch et al., 1992, 2003; Bowen and Bowen, 2008; Baczynski et al., 2013), South America (e.g., Jaramillo et al., 2010), Europe (e.g., Cojan et al., 2000; Schmitz and Pujalte, 2007), Asia (e.g., Bowen et al., 2002; Chen et al., 2014), India (e.g., Samanta et al., 2013), and Australia (e.g., Greenwood et al., 2003). Of these, the Bighorn Basin of Wyoming preserves the most detailed, richly fossiliferous, and best studied terrestrial record of the PETM. Here the PETM corresponds with rapid turnover in both plants and mammals, as the Paleocene flora is replaced by a dry tropical flora (Wing et al., 2005) and the first representatives of several mammalian clades disperse among the Holarctic continents (Gingerich, 2006). The "dwarfing" of about 40% of mammalian lineages also occurred during the PETM (Gingerich, 1989; Clyde and Gingerich, 1998; Secord et al., 2012). The hydrologic cycle was also strongly affected (Wing et al., 2005; Foreman et al., 2012; Kraus et al., 2013; Foreman, 2014; Baczynski et al., 2017). A comprehensive summary of terrestrial environmental changes associated with the PETM can be found in McInerney and Wing (2011). In contrast to the PETM, terrestrial records of the post-PETM hyperthermals are limited. They include carbon isotope records from coal exposures in NE China (Chen et al., 2014) and western India (Clementz et al., 2011; Samanta et al., 2013; Agrawal et al., 2017), as well as records from paleosol carbonates preserved in floodplain deposits from the McCullough Peaks region in the central Bighorn Basin (Abels et al., 2012, 2016; D'Ambrosia et al., 2017). Four post-PETM hyperthermals (ETM2, H2, I1 and I2) are preserved in the McCullough Peaks sequence and this area offers one of the best opportunities for constructing a highly detailed terrestrial record, that can also be compared with marine and terrestrial records of the PETM and post-PETM hyperthermals worldwide. The McCullough Peaks fauna, however, is limited compared to other parts of the Bighorn Basin, complicating direct correlation between hyperthermals and faunal change.

Records of the PETM show that terrestrial proxies generally record a larger magnitude CIE than marine proxies, leading some to consider the terrestrial record "amplified" (Bowen et al., 2004). In marine carbonate records of the PETM, the CIE generally ranges from ~2–4 ‰ (McInerney and Wing, 2011). In terrestrial records, the PETM CIE ranges from ~3–7 ‰ depending upon the proxy used and can show considerable spatial variability depending on local environmental differences (Bowen and Bowen, 2008). Of the terrestrial $\delta^{13}C$ proxies, paleosol carbonates record the largest CIE, generally ranging from ~3–7 ‰ (e.g., Koch et al., 2003; Bowen et al., 2004; Bowen and Bowen, 2008), with a mean of ~5.5 ‰ (McInerney and Wing, 2011). A direct

comparison of marine and paleosol carbonate records indicates that the CIE is on average 2.8–3.0 ‰ greater in paleosol carbonates (McInerney and Wing, 2011).

Detailed paleosol carbonate records of the post-PETM hyperthermals are currently limited to McCullough Peaks, but also seem to show a larger magnitude CIE relative to the marine record. Marine benthic carbonate records of the ETM2 and H2 CIEs are ~1.4–1.5 ‰ and 0.8 ‰, respectively (Stap et al., 2010; Barnet et al., 2019), whereas the terrestrial ETM2 and H2 records from soil carbonates in McCullough Peaks are ~3.8 ‰ and ~2.8 ‰ (Abels et al., 2012, 2016; D'Ambrosia et al., 2017). No terrestrial organic carbon records exist for these hyperthermals from the Bighorn Basin, although bulk organic carbon records from India and China have an average magnitude of ~2.7–3.5 ‰ for ETM2 and ~2.5 ‰ for H2 (Chen et al., 2014; Agrawal et al., 2017). Moreover, there is debate surrounding the scaling relationship between the amplitude of the PETM and post-PETM CIEs, with some arguing for a consistent linear relationship and therefore common source (e.g., Chen et al., 2014) and others arguing that the post-PETM CIEs appear to scale linearly with each other, but not with the PETM, potentially suggesting a different triggering mechanism for the later hyperthermals (Abels et al., 2016).

The cause of the apparent "amplification" in terrestrial CIEs is not fully understood, although increased soil productivity (Bowen, 2013), increased humidity (Bowen et al., 2004; Bowen and Bowen, 2008), increased carbon isotope discrimination by plants under higher atmospheric *p*CO2 conditions (Schubert and Jahren, 2013), and the loss of gymnosperms in the PETM (Smith et al., 2007), which have higher $\delta^{13}C$ values than angiosperms, have been invoked as potential mechanisms. Alternatively, increased dissolution during hyperthermals could produce a muted CIE signal in some marine records relative to actual atmospheric $\delta^{13}C$ shifts (Zachos et al., 2005). The paucity of terrestrial records of post-PETM hyperthermals outside of the McCullough Peaks area makes it difficult to understand how these records vary spatially and to compare CIE magnitudes between the terrestrial and marine realms.

Deleted: this

Deleted: the true

### 1.3 Mammal response to hyperthermals

The PETM coincides with one of the most profound phases of mammal turnover during the Cenozoic, marked by the first appearances of several clades including: Perissodactyla, Artiodactyla, Euprimates, and Hyaenodontidae (e.g., Rose, 1981; Gingerich, 1989, 2003, 2006; Koch et al., 1992; Clyde and Gingerich, 1998; Hooker, 1998; Rose et al., 2012). These taxa disperse among North America, Europe, and Asia during the PETM, but their areas of origin are uncertain (e.g., Bowen et al., 2002; Clyde et al., 2003; Smith et al., 2006; Morse et al., 2019). Several groups also demonstrate transient "dwarfing" during the PETM (Gingerich, 1989; 2006; Clyde and Gingerich, 1998; Strait, 2001; Chester et al., 2010), with minimum body sizes corresponding to peak warming in Bighorn Basin equids (Secord et al., 2012), the only clade described in stratigraphic detail through the PETM.

Previous work on mammal faunas from post-PETM hyperthermals in McCullough Peaks suggests that mammal body size decreased during ETM2 in at least two lineages, though the fauna did not show major reorganization as is seen during the PETM (Abels et al., 2012; D'Ambrosia et al., 2017). However, PETM reorganization may largely be related to intercontinental and intracontinental immigrants making first appearances, while there is no strong evidence for such immigrants appearing

around the time of ETM2 or H2 (Woodburne et al., 2009; Chew, 2015). Until now, the lack of abundant fossil mammals tied closely to the stable isotope record has precluded a detailed assessment of mammal faunal change through these hyperthermals. Chew (2015) identified two distinct pulses of increased turnover and diversity, known as faunal events B–1 and B–2, in mammal assemblages from the Fifteenmile Creek area in the south-central Bighorn Basin. In contrast to the PETM, faunal change during these events was lower in magnitude and driven by increased beta, rather than alpha, diversity. Moreover, the number of first appearances was roughly equal to the number of last appearances and no known intercontinental immigrant taxa arrived during the B–1 and B–2 events. Additionally, abundance shifts during these events appear to have favored smaller bodied species (Chew, 2015). Species richness parameters used by Chew (2015) were significantly correlated to sample sizes, potentially indicating some sample size bias. Chew and Oheim (2013), however, found similar increases in beta richness after correcting for sample variation in the same study area, suggesting that these patterns are independent. Chew (2015) suggested that the ETM2 and H2 hyperthermals were potential drivers of faunal change during events B–1 and B–2, based on inferred temporal overlap of these events with geochemical records from other parts of the basin. Preliminary geochemical work in this region, however, did not identify any clear CIEs in this interval that would confirm this connection (Koch et al., 2003).

Our work presents new, high-resolution carbon isotope records from paleosol carbonates through the Fifteenmile Creek area in the south-central Bighorn Basin. This allows, for the first time, the extensive fossil mammal records from this area to be tied directly into the isotope stratigraphy of post-PETM early Eocene hyperthermals. The results offer a direct test of the hypothesis that faunal turnover events B–1 and B–2 are correlated with the ETM2 and H2 hyperthermals (Chew, 2015). This new record also adds to the terrestrial stable isotope record of post-PETM hyperthermals in the Bighorn Basin, allowing for better spatial characterization of these events.

## 2 Geological setting

The Bighorn Basin is a Laramide structural basin located in northwest Wyoming. Uplift of the Beartooth, Pryor, Bighorn, and Owl Creek mountains resulted in sediment accumulation in the basin during the early Paleogene (Gingerich, 1983; Kraus, 1992). The early Paleogene basin axis was located near the western margin of the basin and sediment thickness generally decreases going from the northwest to southeast within the basin (Parker and Jones, 1986). Regional differences in subsidence area potentially due to activation of east–west trending buried faults (Kraus, 1992). The lower Eocene Willwood Formation represents a fluvial depositional system, and it is typified by paleosols of varying maturity, channel sandstones, crevasse-splay deposits, and localized carbonaceous shales (Kraus, 1992, 1997; Bown and Kraus, 1993). The most complete published record of early Eocene hyperthermals comes from the McCullough Peaks area. This area experienced rapid subsidence during this time and the Willwood Formation here is characterized by a thick sequence of relatively immature paleosols.

The Fifteenmile Creek area of the Bighorn Basin is located ~80 km southeast of McCullough Peaks and, in contrast to the McCullough Peaks, it is characterized by having more mature paleosols, as well as more channel and cut-and-fill deposits associated with slower subsidence and aggradation. The region has produced an extensive collection of nearly 1000 mammal

Deleted: southern
Deleted: there were
Deleted: arriving
Deleted: identified
Deleted: as
Deleted: their
Deleted: fossil-rich
Deleted: southern
Deleted: ),
Deleted: with r
Deleted: Near
Deleted: , the basin

fossil localities that have been tied to a 700 m thick composite stratigraphic section (Bown et al., 1994). Previous work in the area suggested that the stratigraphic interval containing the ETM2 and H2 hyperthermals was between 380 and 455 meters in the Bown et al. (1994) composite section (Chew, 2015). This interval occurs in the *Bunophorus etsagicus* mammalian interval zone (Wa-5), following the last occurrence of *Haplomylus speirianus*. The *Bunophorus etsagicus* interval zone contains the faunal event Biohorizon B (Schankler, 1980; Bown et al., 1994; Chew, 2009), which occurs just below ETM2 and H2 in sections farther north (Abels et al., 2012; D'Ambrosia et al., 2017). The Chron C24r – C24n.3n geomagnetic polarity reversal provides additional support for this interval containing ETM2 and H2. In McCullough Peaks and other records around the world, the C24r – C24n.3n reversal occurs just above ETM2 (Lourens et al., 2005; Abels et al., 2012; D'Ambrosia et al., 2017). Thus, ETM2 is closely bracketed by Biohorizon B below and the Chron C24r – C24n.3n polarity reversal above. Magnetostratigraphic work from Elk Creek Rim, about 20 km north of the Fifteenmile Creek sections studied here, placed the C24r – C24n.3n reversal at the ~450 meter level of the Bown et al. (1994) composite section, ~70 meters above Biohorizon B (Clyde et al., 2007; however see Tauxe et al., 1994 for earlier magnetostratigraphic interpretation). Based on these constraints, we constructed detailed carbon isotope datasets from stratigraphic sections along Fifteenmile Creek that span the critical interval between Biohorizon B and the C24r – C24n.3n reversal to identify ETM2 and H2.

**Deleted:** in

**Deleted:** ,

**Formatted:** Font: Italic

**Deleted:** follows

**Deleted:** the mammal

**Deleted:** and the first occurrence of *Bunophorus estagicus*

**Deleted:** associated with

**Formatted:** Font: Italic

**Deleted:** ,

**Deleted:** meaning

**Deleted:** and determine their correlation to mammal faunal changes.…

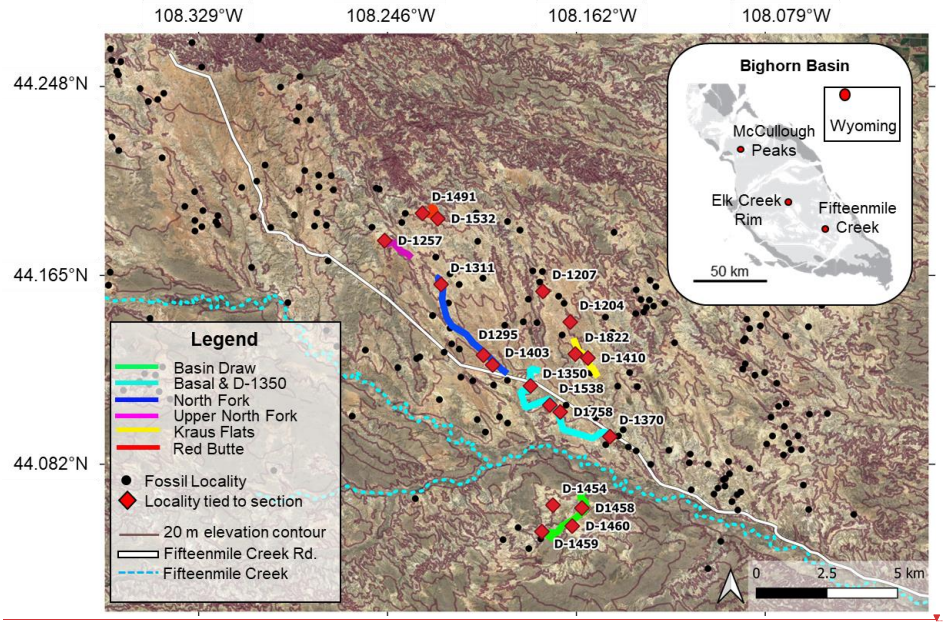


**Figure 1: Map of the Fifteenmile Creek area of the Bighorn Basin, WY showing mammal fossil localities (black dots) and carbon isotope sections (colored lines), overlain onto satellite imagery. Fossil localities that were sampled directly or tied to these sections via lithological tracing are shown as red diamonds and labelled with locality numbers. Inset map shows the location of the Fifteenmile Creek area relative to McCullough Peaks within the Bighorn Basin. Shading key for the inset map: dark grey = Fort Union Formation (Paleocene), light grey = Willwood Formation (Eocene), white = Quaternary alluvium. Basemap source: Google Earth © 2021. More detailed maps of the indivudual sections are available in Figures A1-A6.**

## 3 Methods

### 3.1 Field methods

Pedogenic carbonate nodules were collected from six primary stratigraphic sections that span the target interval (Fig. 1). All samples were collected from fresh, unweathered rock and at least three nodules were analyzed from each sampling site, when possible. Sample sites were chosen to ensure at least a 1-meter sampling resolution, where possible, and levels near a potential CIE were sampled at a higher resolution during subsequent field seasons. Samples were collected from > 30 cm below the upper surface of B horizons in variegated paleosols. At this depth, soil $CO_2$ is primarily plant-respired and will track atmospheric $CO_2$ $\delta^{13}C$ (Cerling, 1984). The relative stratigraphic positions of sampling sites and fossil localities were measured in local sections using a Jacob's staff and bed tracing. These sections were correlated to the composite stratigraphic section of



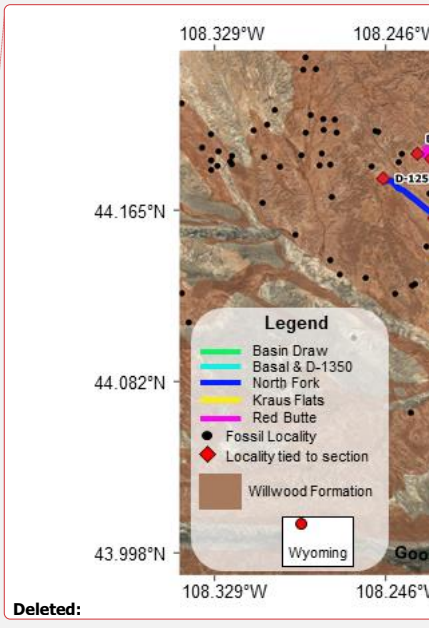


Deleted:

Deleted: the Willwood Formation (brown shading),

Deleted: Willwood Formation extent is from Green and Drouillard (1994). Note that some Willwood Formation exposures are found in areas mapped as Quaternary alluvium (not shaded).

Deleted: M

Deleted: s: USGS (Green and Drouillard, 1994), and

Deleted: Materials and methods

Deleted: 3.1 Pedogenic carbonate¶
Pedogenic carbonate nodules precipitate from soil $CO_2$, a mixture derived from $CO_2$ respired from plants and microorganisms, atmospheric $CO_2$, and dissolved soil parent material (Zamanian et al., 2016). Carbon isotope fractionation in the atmosphere–plant–soil–carbonate system is well characterized (e.g., Cerling, 1984; Farquhar et al., 1989; Cerling and Quade, 1993; Koch, 1998; Wy et al., 2005; Wynn, 2007). At depth (> 30 cm), where most pedogenic carbonate nodules form, soil $CO_2$ is primarily plant respired (Cerling, 1984) and carbonate carbon isotope variation h been shown to closely follow the local vegetation and soil organi matter (Cerling and Quade, 1993). Fractionation during photosynthesis in C3 plants leads to an average $\delta^{13}C$ value of pla tissues depleted in $^{13}C$ by ~ -19.5 ‰ relative to the atmosphere (Koch, 1998), although several factors can affect the degree of

Deleted: 2

Deleted: five

Bown et al. (1994) by using the composite stratigraphic levels (hereafter referred to as "Bown composite meter levels" or BCM) of fossil localities that were measured into our sections and using our Jacob's staff measured thickness to determine BCM levels for the rest of the section. Because of the difficulty with tracing individual beds in this low relief area with spatially dispersed outcrops, we employed a second method to correlate between the main sections using local elevation. Elevations were collected using a Trimble GeoXT 6000 handheld differential GPS (dGPS) paired with a Trimble Tornado external dual-frequency antenna. Elevations were collected from sample sites and from important stratigraphic markers (e.g., marker beds and fossil producing horizons) in every section (Appendix A). Elevation is a reasonable proxy for stratigraphic level in the Fifteenmile Creek area since the dip is close to 0°. Checks on local dips were made by tracing well exposed beds using the dGPS and by shooting a horizontal line between exposures of a marker bed along the section transect. If local differences in dip along the transect were detected, adjustments to dip were made on the Jacob Staff's clinometer. Postprocessing of dGPS data was done using the Trimble Pathfinder Office and Terra Sync Software. After processing, the elevations typically had an accuracy of < 50 cm.

A total of 18 fossil localities, which include more than 4500 identified fossil mammal specimens, were directly tied to the six primary local stratigraphic sections from which isotope samples were collected (Fig. 1) and used to correlate these sections to BCM levels. Three shorter sections were also sampled for carbonate nodules, one near the main Basin Draw section (through fossil locality D–1454), and two located near the Kraus Flats and Red Butte sections (through localities D–1207 and D–1532, respectively) (Appendix B).

### 3.2 Laboratory methods

Individual nodules were polished using a diamond lap wheel and were visually inspected to identify any primary, secondary, or altered textures. Micritic calcite and sparite were sampled for stable isotope analysis. Micrite is generally interpreted to represent a primary phase formed by precipitation directly from soil $CO_2$, and thus is appropriate for paleoclimate reconstruction (Bowen et al., 2001). Sparite samples were also drilled from a subset of nodules to compare stable isotope values of primary and secondary components (e.g., Bowen et al., 2001; Snell et al., 2013). Sparite in paleosol carbonate nodules generally forms in veins and septarian-style cracks in the nodules. It is thought to precipitate from fluids after deep burial at high temperatures, resulting in lower $\delta^{18}O$ values than the original soil water $\delta^{18}O$ (Bowen et al., 2001; Snell et al., 2013). All stable isotope ratios are reported in delta (δ) notation as per mil (‰) deviation relative to the Vienna Pee Dee Belemnite (VPDB) standard, where $\delta = ([(R_{Sample} / R_{Standard}) - 1] \times 1000)$, and R is the ratio of the higher mass isotope to the lower mass isotope.

Analyses of $\delta^{13}C$ and $\delta^{18}O$ values were done at the University of Michigan Stable Isotope Laboratory (UMSIL) using a Thermo Finnegan MAT253 stable isotope ratio mass spectrometer attached to a Kiel IV automated preparation device, and at the University of Colorado Boulder Earth Systems Stable Isotope Laboratory (CUBES–SIL) using a Thermo Delta V continuous flow stable isotope ratio mass spectrometer attached to a GasBench II gas preparation device. Repeated measurements of in-house standards yield precision of ± 0.1 ‰ or better for both $\delta^{13}C$ and $\delta^{18}O$ in both laboratories, although overall uncertainties

Deleted: included in the
Deleted: the
Deleted: infer
Deleted: of correlation
Deleted: to develop an independent stratigraphic framework.
Deleted:
Deleted: .
Deleted: 3.3 Mammal fossil localities¶
Deleted: that
Deleted: five
Deleted: the
Deleted: away from
Deleted: A
Deleted: 4

are likely slightly larger than this in carbon isotopes due to extrapolation of the standard correction lines beyond the lowest standard values for both labs (Appendix C). Data correction and calculations from CUBES–SIL were done using in-house R scripts that utilized Tidyverse and IsoVerse R packages (R Core Team, 2019; Wickham et al., 2019; Kopf et al., 2021). Powder from a subset of 10 micrite samples was homogenized and replicates were sent to UMSIL and CUBES–SIL to identify if there were differences between the two labs. $\delta^{13}C$ and $\delta^{18}O$ values that were measured at UMSIL were then corrected to the CUBES–SIL values based on these replicate samples (Appendix C).

CIE magnitudes were calculated by detrending the data to account for long-term early Paleogene trends, then taking the difference between the detrended $\delta^{13}C$ background values and the values from the body of the CIEs, following the method of Abels et al. (2016). $\delta^{13}C$ values were averaged from each stratigraphic level prior to calculating the magnitude and the mean peak excursion values from each section were also averaged to facilitate comparisons to other records and account for local spatial heterogeneity.

## 4 Results

### 4.1 Stable isotopes

A total of 789 carbonate samples from the Fifteenmile Creek area were analyzed for $\delta^{13}C$ and $\delta^{18}O$ (Figs. 2 and 3). $\delta^{13}C$ values for micritic carbonate samples (n = 770) range from -16.4 ‰ to -8.7 ‰ (mean = -11.0 ‰). Micrite $\delta^{18}O$ values range from -16.6 ‰ to -6.5 ‰ (mean = -9.3 ‰). Sparite samples (n = 19) display $\delta^{13}C$ values between -21.2 ‰ and -9.5 ‰ (mean = -12.6 ‰) and $\delta^{18}O$ values between -23.4 ‰ and -8.6 ‰ (mean = -14.8 ‰) (Fig. 2). Twelve samples were removed due to relatively low weight percent carbonate (< 50 %). Low weight percent carbonate introduces the possibility that the carbonate in these samples does not reflect pedogenesis, or they could be higher porosity samples that were more susceptible to alteration. Fifty percent is a somewhat conservative cutoff that only retains samples that are majority carbonate. Considering only sampling sites with at least three nodules, the mean within–site range in $\delta^{13}C$ is 0.7 ‰ but can be up to 3.2 ‰. The mean within–site range in $\delta^{18}O$ is 0.9 ‰ and up to 5.8 ‰. Together, the within–site range in both $\delta^{13}C$ and $\delta^{18}O$ are generally < 1 ‰.

It is possible that small amounts of unrecognized spar or areas of recrystallization were drilled with the micrite, which could contribute to the large spread in $\delta^{18}O$ towards more negative values (Fig. 2). As such, samples with $\delta^{18}O$ values greater than 2σ below the mean micrite $\delta^{18}O$ value (-11.7 ‰) were identified as potentially incorporating a secondary spar phase and are shown as such in Figs. 3 and 4. Secondary recrystallization in a closed system does not affect carbon isotopes to the same extent as oxygen isotopes (Cerling, 1984), suggesting that partially recrystallized samples may still record CIEs reliably. Two stratigraphic levels from the base of the Basin Draw section have anomalously low $\delta^{13}C$ values (up to -16.4 ‰) that fall outside of the typical range for early Eocene pedogenic carbonate from this region and could incorporate some mixing with sparite, particularly given their relatively low $\delta^{18}O$ values (down to -12.1 ‰).

Replicate samples that were analyzed by the two laboratories (n = 10) show that $\delta^{13}C$ values differed by up to 0.7 ‰ (mean = 0.4 ‰, standard deviation = 0.3 ‰) while $\delta^{18}O$ values differed by up to 0.6 ‰ (mean = 0.3 ‰, standard deviation = 0.2 ‰).

Deleted: B

Deleted: B

Deleted: had

Deleted: up

Greater differences between the two labs are consistently associated with more negative values, and $\delta^{13}C$ and $\delta^{18}O$ values produced in the CUBES–SIL lab are generally more negative than values from the UMSIL. These offsets are likely due to differences in standardization between the labs and this relationship was used to correct the UMSIL data to the CUBES–SIL values (Appendix C). This laboratory offset is within the range of observed within–site variation described above, indicating that the offset is not likely to affect the stratigraphic interpretations relevant to this study.

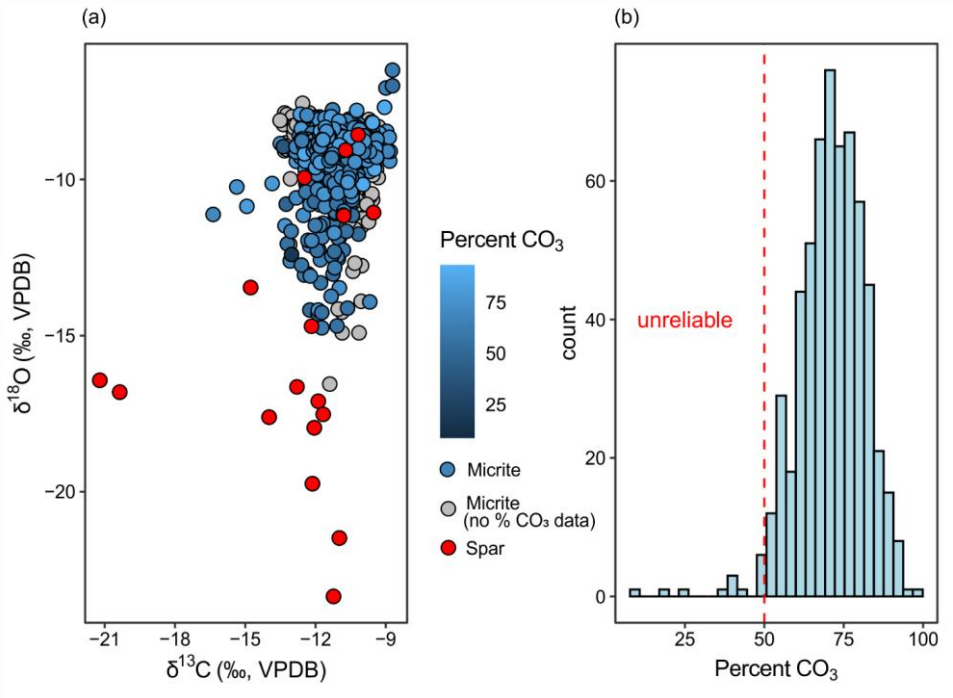


**Figure 2: (A) $\delta^{13}C$ and $\delta^{18}O$ for sparite and micrite samples measured from Fifteenmile Creek. Samples analyzed in the CUBES–SIL lab are colored according to their weight % $CO_3$. Samples analyzed by the UMSIL lab are shown in grey. (B) Weight percent carbonate from the CUBES–SIL samples. Thirteen samples with less than 50% $CO_3$ were considered unreliable and were removed.**

### 4.2 Carbon isotope excursions

Carbon isotope excursions were identified as places where site mean $\delta^{13}C$ values were less than -12 ‰ and the values show a clear decrease and return to background levels (between about -9 ‰ and -11 ‰, mean background $\delta^{13}C$ = -10.3 ‰), Places

Deleted: B

Formatted: Superscript

where single samples or site means were less than -12 ‰ and were surrounded by background values above and below, or places where the return to background values was not captured were not considered CIEs. CIEs were identified in all six sections. In Basin Draw, there is a CIE between ~45 to 55 m level there is a CIE with minimum $\delta^{13}C$ site values reaching -12.0 ‰. The lower ~35 m of this section are characterized by noisy $\delta^{13}C$ records that are more negative than the average background value, but do not show a clear CIE pattern. In the Basal/D-1350 section, there is a well-defined CIE between the 30 – 45 m level with a minimum mean $\delta^{13}C$ site value of -13.3 ‰. Two CIEs are recorded in the Kraus Flats section, one between ~ 0 – 25 m level (minimum site $\delta^{13}C$ = -12.8 ‰) and another between ~35 – 45 m level (minimum site $\delta^{13}C$ = -12.7 ‰). The base of the North Fork section includes sites with relatively low $\delta^{13}C$ values (minimum site $\delta^{13}C$ = -13.3 ‰) that return to background levels around the 20 m level. Based on field correlations and close geographic proximity with the Basal/D-1350 section (Appendix A), we interpret this negative shift to be equivalent to the excursion at the top of the Basal/D-1350 section. This interpretation is also supported by composite meter levels from Bown et al. (1994), which indicate that stratigraphic levels at the top of the Basal/D-1350 section should be equivalent to levels in the bottom of the North Fork section. Thus, we consider the negative shift in values at the bottom of the North Fork section to represent a CIE, even though the onset is not captured here. The ~20 – 30 m level in North Fork also records a smaller CIE (minimum site $\delta^{13}C$ = -12.2 ‰), though the record is less clear. The Upper North Fork section captures the onset and recovery of one CIE, with a minimum site $\delta^{13}C$ of -12.2 ‰ at the 12 m level. The Red Butte section records a CIE in the 0 – 20 m level (minimum site $\delta^{13}C$ = -12.2 ‰) and also appears to capture the onset of a second CIE in the upper 10 m of the section. Because the recovery and potentially even the minimum values of this uppermost excursion aren't present in our record, we haven't identified this as a CIE, although future work may find that this a higher CIE.

In addition to the correlation between the Basal/D-1350 CIE and the lowest CIE in North Fork, measured sections and bed traces indicate that the Upper North Fork CIE is stratigraphically higher than the second CIE in the North Fork section. Bed traces between the Upper North and Red Butte sections also indicate that the CIE in the Upper North Fork and Red Butte sections are equivalent (Appendix A). Both the Upper North Fork and Red Butte CIEs occur in lateral equivalents of the same yellow siltstone. The Kraus Flats section was not tied directly to another section by bed tracing. However, the carbon isotope stratigraphy and general placement of this section within composite framework of Bown et al. (1994) support a correlation between the two CIEs in Kraus Flats and the two CIEs in North Fork. The Basin Draw section was also not correlated to another section by tracing beds. The BCM levels of fossil localities in the upper part of this section support correlation to the higher CIE in North Fork and Kraus Flats however, no lower CIE is clearly preserved in this section. Additionally, differential GPS elevations suggest that this CIE may line up better with the lower CIE in the North Fork and Kraus Flats sections (Fig. 4). For these reasons, the Basin Draw CIE remains uncorrelated. Together these data indicate that three distinct CIEs are fully recorded in the field area. The lowest CIE ("CIE1") occurs in the Basal/D-1350, North Fork, and Kraus Flats sections. The middle CIE ("CIE2") occurs in the North Fork and Kraus Flats sections and the highest CIE ("CIE3") occurs in the Upper North Fork and Red Butte sections.

**Deleted:** Three stratigraphic intervals have consistently low carbon isotope values (< ~ -12 ‰) relative to background levels (between about -8 ‰ and -12 ‰, mean background $\delta^{13}C$ = -10.3 though the precise BCM levels at which these intervals occur var among the sections (Fig. 4a). The lowest excursion occurs betwe the 405–430 BCM levels, the middle excursion between the 430- 455 BCM levels, and the highest excursion between the 460–500 BCM levels. When the data are plotted against dGPS elevation, t variability in their stratigraphic position is reduced with the lowe excursion occurring between 1320–1340 m in elevation, the mid excursion between 1340–1355 m, and the highest excursion betw 1370–1405 m (Fig. 4b). Oxygen isotopes do not show any clear differences between hyperthermal and non-hyperthermal interval (Appendix C). This is consistent with observations that changes i pedogenic carbonate $\delta^{18}O$ during the PETM are muted compared the $\delta^{13}C$ record, possibly due to temperature fractionation in the carbonate acting in an opposing direction to temperature fractionation in the atmosphere (e.g., Koch et al., 2003). ¶
The magnitudes of the CIEs also vary, both across the different sections and from one CIE to another. The average magnitude of stratigraphically lowest CIE is 2.4 ‰, with minimum mean $\delta^{13}C$ values ranging from -13.3 ‰ to -12.0 ‰ in different sections. Th average magnitude of the middle CIE is 1.3 ‰, with minimum δ values of -12.7 ‰ and -12.2 ‰. The average magnitude of the stratigraphically highest CIE is 1.6 ‰ with minimum $\delta^{13}C$ values -12.2 ‰.…

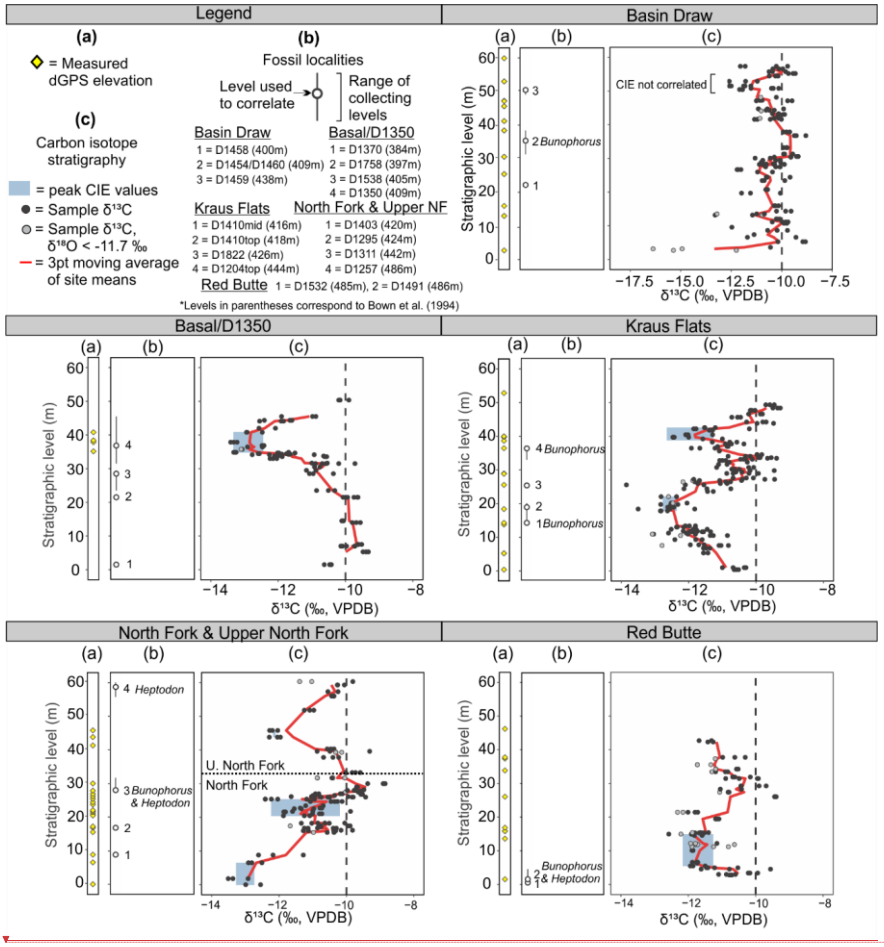


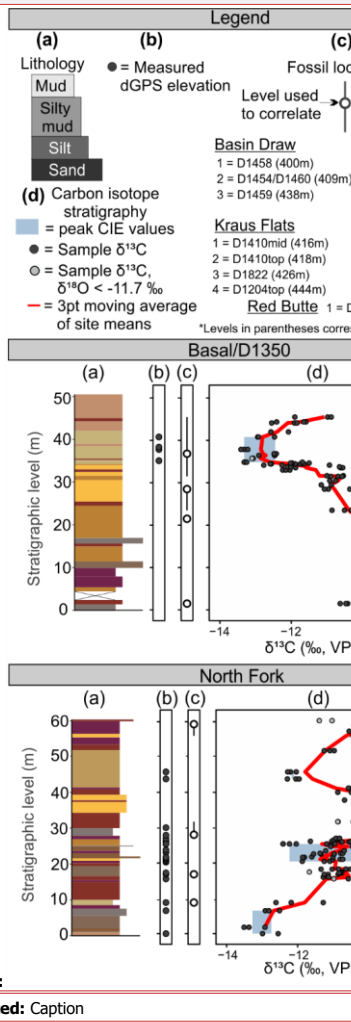


**Figure 3: Carbon isotope data from pedogenic carbonate nodules for Fifteenmile Creek sections. (a) Stratigraphic levels where dGPS elevations were collected. (b) Fossil localities that were sampled within the section. Open points correspond to the Bown et al. (1994) composite meter level for the locality and main collecting level. Lines show ranges of collecting levels. Fossil localities with *Bunophorus* are Wa5 or above. Localities with *Heptodon* are Wa6 or above. (c) Carbon isotope stratigraphy. Points represent measurements for individual nodules. Red lines are a three-point moving average through the mean values from a sampling site and blue shading shows range of peak values used to calculate CIE magnitudes. Note that the CIE at ~45 m in the North Fork/Upper North Fork sections includes a small range of ~-12 ‰ values.** Black dashed lines at -10 ‰ show typical background value for Fifteenmile Creek.

Deleted:

Formatted: Caption

Deleted: 3…: Carbon isotope data from pedogenic carbona… nodules and lithology …or Fifteenmile Creek sections. (a) Lithostratigraphy, colors represent outcrop color. (b) Stratigraphic levels where dGPS elevations were collected. (b…

Formatted

Deleted: d

Formatted

Deleted: ¶

## 4.3 Stratigraphy

Placing the individual measured sections into the BCM and elevation frameworks can help confirm the field-based correlations (Fig. 4). CIE1 occurs between the 405 – 430 BCM levels, CIE2 between the 430–455 BCM levels, and the CIE3 between the 460 – 500 BCM levels (Fig. 4a). When the data are plotted against dGPS elevation, CIE1 occurrs between 1320 – 1340 m in elevation, CIE2 between 1340 – 1355 m, and CIE3 between 1370 – 1405 m (Fig. 4b). Oxygen isotopes do not show any clear differences between hyperthermal and non-hyperthermal intervals (Appendix D). This is consistent with observations that changes in pedogenic carbonate $\delta^{18}O$ during the PETM are muted compared to the $\delta^{13}C$ record, possibly due to temperature fractionation in the carbonate acting in an opposing direction to temperature fractionation in the atmosphere (e.g., Koch et al., 2003). The magnitudes of the CIEs also vary, both across the different sections and from one CIE to another. The average magnitude of CIE1 is 3.1. The average magnitude of CIE2 is 1.7 and the average magnitude of CIE3 is 2.1 ‰.

The measured thicknesses of the local sections are different than the thicknesses from BCM levels and those inferred from elevation (Fig. 4). The Basin Draw section (55 m thick) is shortened to 41 m in the elevation framework and stretched to 64 m in the BCM framework. The Basal/D-1350 section (49 m thick) maintains a similar thickness in the elevation framework and is shortened to 38 m in the BCM framework. The Kraus Flats section (49 m thick) is shortened to 31 m in the elevation framework and stretched to 55 m in the BCM framework. The Red Butte section (40 m thick) maintains similar thicknesses in both the BCM and elevation frameworks. The North Fork and Upper North Fork sections were correlated to each other using a bed trace in the field (Figs. 3, A4, and A5). The thickness measured for both sections together, based on this bed trace, is ~60 m (Fig. 3), 76 m separate the base of the North Fork section and the top of the Upper North Fork section in the elevation framework and there is 75 m separating them in the BCM framework (Fig. 4). See Appendix A for elevation and fossil locality tie points used in each section.

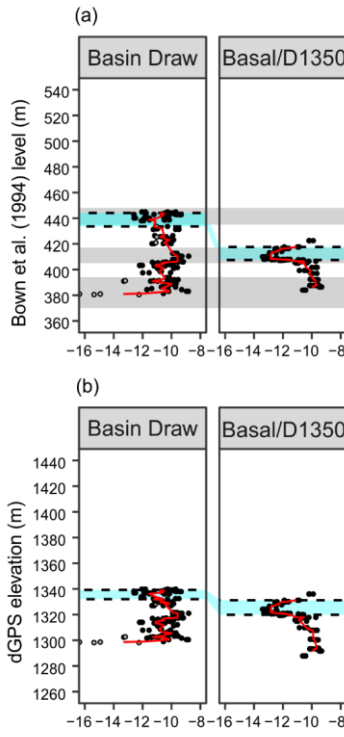


**Deleted:**

**Formatted:** Justified

**Deleted:** **Figure 4: Carbon isotope data for Fifteenmile Cre sections shown (a) using the Bown et al. (1994) equivalent me level, and (b) differential GPS elevation. The stratigraphicall lowest, middle and highest carbon isotope excursions are outlined by the blue, yellow and red shading, respectively. Th stratigraphic intervals associated with the faunal events described in Chew (2015) are shown as grey shaded regions i the top panel. Points represent measurements for individual nodules. Red lines are a three-point moving average through mean values from a sampling site.¶**

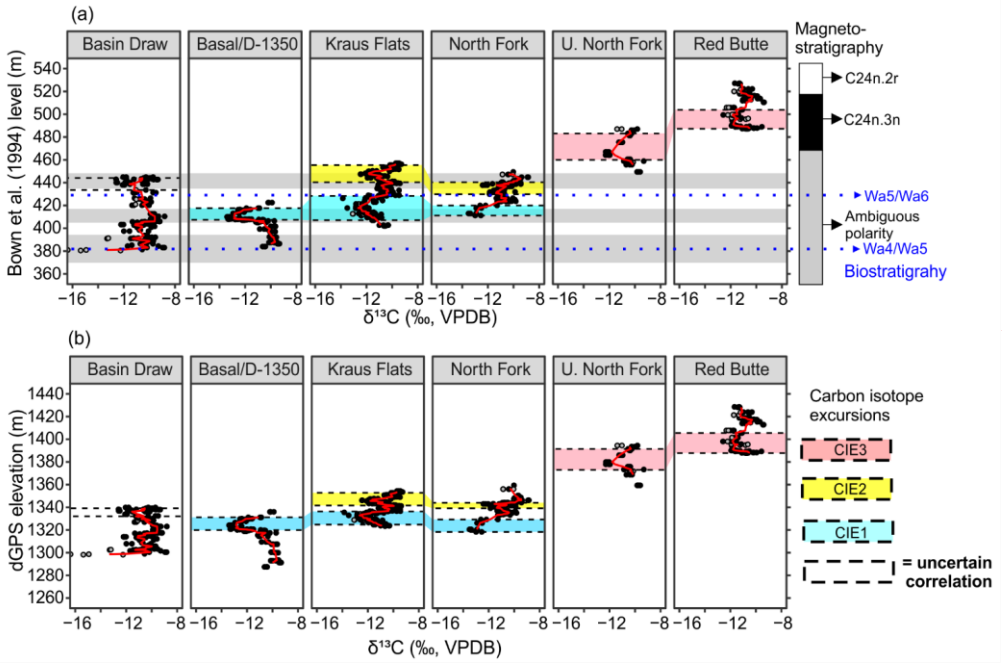


**Figure 4: Carbon isotope data for Fifteenmile Creek sections shown using the (a) Bown et al. (1994) equivalent meter level, and (b) differential GPS elevation. The stratigraphically lowest, middle and highest carbon isotope excursions are outlined by the blue, yellow and red shading, respectively. The stratigraphic intervals associated with the faunal events described in Chew (2015) are shown as grey shaded regions in the top panel, along with faunal zone boundaries (blue dotted lines) based on Bown et al. (1994). Magnetostratigraphy is based on Clyde et al. (2007), partly reinterpreted from Tauxe et al. (1994). Points represent measurements for individual nodules. Red lines are a three-point moving average through the mean values from a sampling site.**

### 4.4 Fossil Localities

Chew (2015) proposed that the 405 – 417 and 435 – 448 BCM levels could correspond to the ETM2 and H2 hyperthermals, based on the observed changes in mammal diversity and rate of turnover in these intervals. The new Fifteenmile Creek isotope records presented here generally support this hypothesis, with the ETM2 hyperthermal overlapping with the 405 – 417 m interval (faunal event B–1) and H2 overlapping with the 435 – 448 m interval (faunal event B–2) (Figs. 4 and 5). This is especially apparent in the Basal/D–1350, Kraus Flats, and North Fork sections. The D–1350 locality (408 – 410 BCM level), for example, shows a clear CIE consistent with ETM2, and also yields several species that first appear during faunal event B–1 (e.g., *Xenicohippus grangeri*, *Diacodexis secans*, *Didymictis lysitensis*, *Eohippus angustidens*). Localities D–1410 (410 – 418 BCM level) and D–1204 (438 – 444 BCM level), which were tied into the Kraus Flats section, produce faunas that are



Formatted: Keep with next

Formatted: Caption

Moved (insertion) [1]

Deleted: Chew (2015) proposed that the 405–417 and 435–448 BCM levels could correspond to the ETM2 and H2 hyperthermals, based on the observed changes in mammal diversity and rate of turnover in these intervals. The new Fifteenmile Creek isotope records presented here broadly support this hypothesis, with the ETM2 hyperthermal overlapping with the 405–417 m interval (faunal event B–1) and H2 overlapping with the 435–448 m interval (faunal event B–2) (Figs. 4 and 6). This is especially apparent in the Basal/D–1350, Kraus Flats, and North Fork sections north of Fifteenmile Creek. The D–1350 locality (408–410 BCM level), for example, shows a clear CIE consistent with ETM2 and also yields several species that first appear during faunal event B–1 (e.g., *Xenicohippus grangeri*, *Diacodexis secans*, *Didymictis lysitensis*, *Eohippus angustidens*). Localities D–1410 (410–418 BCM level) and D–1204 (438–444 BCM level), which we tied into the Kraus Flats section, produce faunas that are consistent with B–1 (D–1410) and B–2 (D–1204), and also overlap with the ETM2 and H2 intervals, respectively. However, some localities show small offsets from their predicted position relative to the CIE record. Locality D–1311 (442 BCM level), for example, falls within the interval associated with faunal event B–2, but just above the CIE associated with H2. Locality D–1403 (426 BCM level) is within the ETM2 CIE but fell outside of the interval reported to contain faunal event B–1 (Fig. 6).

Formatted: Outline numbered + Level: 2 + Numbering Style: 1, 2, 3, … + Start at: 4 + Alignment: Left + Aligned at: 0" + Indent at: 0.25"

consistent with the B–1 (D–1410) and B–2 (D–1204) faunal events of Chew (2015), and also overlap with the ETM2 and H2 intervals, respectively. However, some localities show small offsets from their predicted position relative to the CIE record. Locality D–1311 (442 BCM level), for example, falls within the interval associated with faunal event B–2, but is just above the CIE associated with H2. Locality D–1403 (420 BCM level) is within the ETM2 CIE but fell outside of the interval reported to contain faunal event B–1 (Fig. 5).

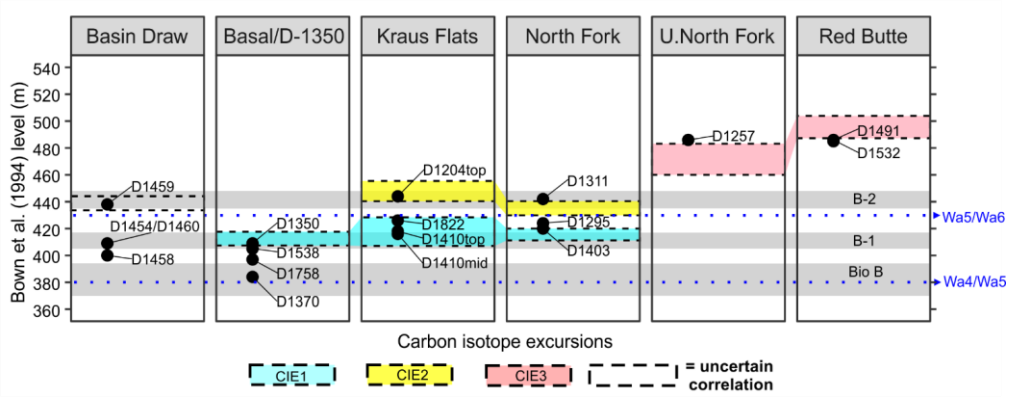


**Figure 5: Selected Fifteenmile Creek fossil localities tied to the Bown et al. (1994) composite section. Shading follows Fig. 4, where stratigraphically lowest, middle, and highest carbon isotope excursions are outlined by blue, yellow and red shading, respectively. The stratigraphic intervals associated with the faunal events described in Chew (2015) are shown as grey shaded regions. Points for the fossil localities incorporate some stratigraphic uncertainty and averaging of collecting levels discussed in the text. Faunal zone boundaries are shown as blue dotted lines. Wa5/Wa6 boundary is based on Bown and Rose (1987). For more detailed ranges of collecting levels associated with the localities, see Fig. 3.**

## 5 Discussion

### 5.1 Stratigraphic correlation and uncertainty

Several aspects of the Fifteenmile Creek stratigraphy complicate direct correlation between sections in the study area, including large lateral spacing and relative lack of vertical relief of exposures. To account for this, we used two methods of correlation, traditional bed tracing and correlation to the Bown et al. (1994) composite section (= BCM levels), and elevations based on dGPS to supplement our field observations. Each of these methods of correlation has its own inherent uncertainty. For example, early fossil collecting in the region may not have specified the producing level for each fossil specimen. The BCM levels

Formatted: Normal, No bullets or numbering

Formatted: Caption

Formatted: Outline numbered + Level: 1 + Numbering St 1, 2, 3, … + Start at: 4 + Alignment: Left + Aligned at: 0" Indent at: 0.25"

Formatted: Outline numbered + Level: 2 + Numbering St 1, 2, 3, … + Start at: 1 + Alignment: Left + Aligned at: 0" Indent at: 0.25"

therefore reflect some degree of stratigraphic averaging of fossil horizons. These composite levels also rely on bed tracing, which is difficult to do precisely over long distances in this low-relief terrane. Although the dGPS elevations presented here account for some of this uncertainty in bed tracing, they assume perfectly horizontal bedding and estimates of thicknesses can be erroneous if there are changes in local dip. Although dip is generally close to zero in this area, bed tracing combined with dGPS measurements has highlighted some local variation in bedding attitude in the field area. The elevations also may be affected by variations in paleo-topography, including lateral variation in paleosol thickness due to relative position on the floodplain and channel meander. Paleosol and sandstone thickness can vary on a meter scale in this area, which is larger than the vertical error of the dGPS (~50 cm). Vertical dGPS error on the elevations therefore likely contributes very little to the observed variation among sections. Field correlation between sections has a higher uncertainty of up to 10 m and in some cases was not possible (Appendix A). Correlation between subsections within a section has a much lower uncertainty and is generally < 1 m for shorter bed traces (Appendix A).

Many aspects that complicate stratigraphic correlation in this region are illustrated with the Basin Draw section. This section is located south of Fifteenmile Creek, across from the main portion of the composite section (Fig. 1) making direct lithostratigraphic correlations difficult. Exposures along this section are also spaced far apart and dGPS elevations routinely underestimate thickness compared to bed tracing between exposures here, suggesting that dip and/or paleosol thickness variation may disproportionally affect these longer traces. Further complicating correlation, a large cut-and-fill deposit occurs in the upper portion of the Basin Draw section and fossil locality D–1459 (between ~430–440 BCM level, or 1330–1336 m elevation) is in the cut-and-fill (Fig. A1).

Despite uncertainties, stratigraphic levels for each of the three CIE intervals are in better agreement across the six sections using dGPS elevation, than with BCM levels (Fig. 4). Using elevation, the CIE in the Basin Draw section correlates better with the stratigraphically lowest excursion in other sections, particularly when we exclude the outliers at the base of the section that appear to be diagenetically altered and not associated with a well-defined excursion. The local biostratigraphy rules out the possibility that these basal samples could be capturing the PETM and the very negative carbon and oxygen isotope values are more consistent with diagenesis. The Basin Draw section also does not preserve two clear CIEs, suggesting that the CIE near the top of the section would correlate to the lowest CIE in our record. It should be noted that the faunal analysis of Chew (2015) places the top of the Basin Draw section within faunal event B–2, and therefore predicts that it would overlap with the middle CIE, which is inconsistent with this correlation. Due to the ambiguous correlation between Basin Draw and the other sections, we do not correlate this CIE to either of these CIEs and its correlation remains unresolved.

### 5.2 Identification of post-PETM hyperthermals

To account for the geographic variability in bed thickness described above, the five stratigraphic sections that are north of Fifteenmile Creek (Basal/D-1350, Kraus Flats, North Fork, Upper North Fork, and Red Butte), as well as the shorter sections through fossil localities D-1207 and D-1532, were compiled into a "Fifteenmile Creek Composite Section" (Fig. 6). To create the composite section, the peak negative $\delta^{13}C$ values from each CIE were aligned and the relative spacing between CIEs was

Deleted: they do not account for

Deleted: five

Deleted: (< -14 ‰)

Formatted: Outline numbered + Level: 2 + Numbering St 1, 2, 3, … + Start at: 1 + Alignment: Left + Aligned at: 0" Indent at: 0.25"

Deleted: the

Deleted: ree

Deleted: 5

Deleted: , where

Deleted: are

Deleted: is

scaled to the average of the spacing from the sections where we measured the CIEs together. All stratigraphic thicknesses for the composite section are based on the thicknesses we measured with a Jacob's staff in the field, rather than using BCM levels or elevations. The Jacob's staff measurements offer the least uncertainty for individual sections and isotope values are the best means for correlating between sections for purposes of creating a composite section. These correlations are independently supported by both the BCM and elevation frameworks. Using this composite section, the CIE1 occurs between the ~35 to 55 meter level. CIE2 occurs between the ~57 to 70 meter level. CIE3 occurs between the ~85 to 104 meter level, with some relatively low $\delta^{13}C$ values above this that could possibly represent the onset of a fourth CIE (Fig. 6). We confidently identify CIE1 and CIE2 as the ETM2 and H2 hyperthermals, respectively, based on their position relative to Biohorizon B. Elsewhere in the Bighorn Basin, ETM2 lies just above Biohorizon B (Abels et al., 2012; D'Ambrosia et al., 2017). Biohorizon B occurs at the ~11 meter level in our new composite section, suggesting the lowest CIE that starts at ~35 meters is ETM2 (Fig. 6). Magnetostratigraphic data are consistent with this correlation, as the Chron C24r – C24n.3n polarity reversal is known to lie just above ETM2 and correlates to somewhere in the lower 100 meters of our new composite section (Tauxe et al., 1994; Clyde et al., 2007) (Fig. 6).

Identification of the stratigraphically highest CIEs is more difficult. One possibility is that they represent I1 and the onset of I2. Another possibility is that they correspond to a less well-defined negative CIE between H2 and I1 near the 260 m level in the McCullough Peaks composite section that was attributed to local environmental factors (Abels et al., 2016) (Fig. 6). Barnet et al. (2019) have recently shown a small CIE at roughly the same level in the marine record, suggesting that this could be a global signal. Biostratigraphy does little to help resolve these options, due to the small fossil sample sizes in McCullough Peaks. The magnetostratigraphic record supports correlation of our highest CIEs to I1 and I2, based on the presence of the C24n.3n – C24n.2r reversal near the top of our section which is often recorded just after I2 in other records (e.g., Zachos et al., 2010). It is important to note that our sample sections were not correlated directly to the Tauxe et al. (1994) magnetostratigraphy for Fifteenmile Creek. Instead, the magnetostratigraphy is linked with our data using the BCM levels for both records. Moreover, the magnetostratigraphy we've presented in Fig. 6 is a combination of Clyde et al. (2007), who offer a revised level for the C24r – C24n.3n reversal from Elk Creek Rim ~25 km north, and Tauxe et al. (1994), who constrain the level for the C24n.3n – C24n.2r reversal from Fifteenmile Creek. The stratigraphic spacing between the lower and higher CIEs in our section supports the second scenario (correlation to the poorly defined negative CIE between H2 and I1) supporting the idea that this isotopic signal may be more regional or global in scale (Fig. 6). It is also possible that there is a hiatus in the upper part of the Fifteenmile Creek section or that sediment accumulation rates were much slower in this interval. In either case, CIE3 could represent I1.

Cyclostratigraphic constraints on depositional rates across the basin support correlation of CIE3 to the interval between H2 and I1. Aziz et al. (2008) reported a depositional rate of ~2.5 kyr/m at their Red Butte section, located ~3 km northwest of our Red Butte Section, which is similar to McCullough Peaks rates (Abels et al., 2016). Based on observed differences in sedimentation rates, moving from northwest to southeast in the basin, we expect rates to be slower in the lower part of our section. Our ETM2 and H2 CIEs are separated by ~22 m in both sections where they are measured together and these

**Deleted:** two primary excursions

**Deleted:** were measured

**Deleted:** lowest CIE

**Deleted:** The middle

**Deleted:** The highest CIE

**Deleted:** 5

**Deleted:** the two stratigraphically lowest CIEs

**Deleted:**

**Deleted:** 5

**Deleted:** 5

**Deleted:** and magnetostratigraphy do

**Deleted:** , uncertainty on the position of the C24r – C24n.3n reversal in Fifteenmile Creek, and the overall differences in sediment thickness across the basin (Clyde et al., 2007).

**Deleted:** 5

**Moved (insertion) [2]**

**Deleted:** the stratigraphically highest excursion

**Deleted:**

hyperthermals are thought to be orbitally paced by 100 kyr eccentricity cycles (Barnet et al., 2019). This age constraint provides a depositional rate of ~4.5 kyr/m in the lower part of our section. Based on eccentricity maxima, H2 and I1 are separated by ~300 kyr (Barnet et al., 2019). Assuming this slower sedimentation rate, we would expect to see ~67 m of strata between H2 and I1, which is approximately 3x what we observe (Fig. 6). If we assume depositional rates increase up section toward Red Butte, expected thickness would be even greater. Notably, there is a fairly large discrepancy in stratigraphic thickness between the CIE2 and CIE3 in our composite section, measured with a Jacob's Staff and bed traces, compared with thicknesses estimated from BCM levels and dGPS elevation. Elevation and BCM levels suggest there may be as much as twenty additional meters separating H2 from the next highest excursion in our section (Fig. 4). These excursions were measured in separate sections (North Fork and Upper North Fork) tied together with a long bed trace of 1.6 km (Fig. A4 and A5), which could result in some error. Another source of error could be differences in placement of stratigraphic levels within fossil localities. BCM levels for localities are based on the stratigraphic position of a key fossil bearing bed within a locality, but many localities have several fossil bearing horizons. In most cases, we were uncertain which level was used by Bown et al. (1994) to demarcate a locality's stratigraphic level. Although we are unable to provide a confident reason for this stratigraphic discrepancy, the addition of 20 meters to the distance between H2 and the next highest CIE still falls far short of the expected thickness if the latter represents I1. Better age control is needed for a confident identification of the upper CIE.

### 5.3 Comparison to other post-PETM hyperthermal records

The carbon isotope values vary between Fifteenmile Creek and McCullough Peaks (Fig. 6). In McCullough Peaks, the average magnitude of the ETM2 and H2 CIEs are 3.8 ‰ and 2.8 ‰, respectively. In Fifteenmile Creek, these magnitudes are 3.1 ‰ and 1.7 ‰. The smaller CIE magnitudes in Fifteenmile Creek indicate that these atmospheric perturbations are recorded differently in different parts of the same basin and likely reflect local differences in vegetation structure or soil moisture. The strongest single environmental control on $\delta^{13}C$ values in C3 vegetation is water availability to plants, which accounts for about half of the variability, with plants discriminating less against $^{13}C$ under drier conditions (Ehleringer, 1993; Stewart et al., 1995; Diefendorf et al., 2010; Kohn, 2010, 2016). This suggests that drainage differences between McCullough Peaks and Fifteenmile Creek could contribute to some of the variation between the two records. Abels et al. (2016) found that precipitation change during the post-PETM hyperthermals appears to have been negligible, based on mean annual precipitation estimates using the CALMAG proxy. This contrasts with drier conditions interpreted during the PETM from various soil proxies and fossil leaves (Wing et al., 2005; Kraus et al., 2013; Abels et al., 2016). Paleosol analysis across the Bighorn Basin shows that soil drainage varies significantly even across a small geographic area (e.g., Kraus, 1992, 1997). Secord et al. (2008) inferred vegetation structure based on carbon isotopes in mammalian tooth enamel from the Fifteenmile Creek area and found that vegetation was relatively dense, but that the forests had an open canopy. The "canopy effect," resulting from highly $^{13}C$-depleted leaves in the understory (e.g., Cerling et al., 2004), also appears to be absent in mammalian enamel from the northern Bighorn Basin (Koch et al., 1995) based on the model in Secord et al. (2008). Given the strong control that water availability has on leaf values, this appears to be the most likely cause of differences in absolute $\delta^{13}C$ values and in differences in CIE

**Moved up [2]:** It is also possible that there is a hiatus in the up part of the Fifteenmile Creek section or that sediment accumulati rates were much slower in this interval. In either case, the stratigraphically highest excursion could represent I1.

**Deleted:** It is also possible that there is a hiatus in the upper pa of the Fifteenmile Creek section or that sediment accumulation ra were much slower in this interval. In either case, the stratigraphic highest excursion could represent I1. Additional sampling and be age control are needed to resolve the precise identification of the upper CIEs.

**Deleted:** <#>¶

**Deleted:** The post-PETM hyperthermal record in Fifteenmile Creek differs from the McCullough Peaks record in several ways The spacing between the CIEs is compressed in Fifteenmile Cree relative to McCullough Peaks. In McCullough Peaks, the peak ETM2 and H2 excursions are separated by approximately 32 m whereas they are separated by approximately 23 m in the Fifteen Creek record (Fig. 5). This is consistent with other studies showi lower sediment accumulation rates due to slower subsidence in th southern part of the Bighorn Basin during the early Eocene (Park and Jones, 1986; Clyde et al., 2007). H2 and I1 are separated by approximately 90 m in McCullough Peaks, while only ~22 m separate H2 from the stratigraphically highest CIE in Fifteenmile Creek, supporting the idea that this may not represent I1. ¶

**Deleted:** also

**Deleted:** 5

**Deleted:** 2.4

**Deleted:** 3

**Formatted:** Superscript

**Formatted:** Superscript

magnitude observed here, although differences in floral composition between the two locations cannot be ruled out as contributing to these differences. The slower sediment accumulation in Fifteenmile Creek also means that pedogenic carbonate in this area may have averaged atmospheric carbon isotope values over a longer time period and thus not recorded the minimum excursion values as reliably if minimum atmospheric values lasted only a short time.

Despite having lower magnitudes than the CIEs in McCullough Peaks, the Fifteenmile Creek CIEs are still amplified relative to the marine benthic record, where the average ETM2 and H2 CIEs are ~1.4 ‰ and 0.8 ‰, respectively (Stap et al., 2010). The amplification effect, however, seems to be somewhat variable even in similar stratigraphic records that are only ~80 km apart within the same basin. This supports the hypothesis that some (or all) of the observed difference in magnitudes between marine and terrestrial CIEs is due to local environmental or time averaging effects.

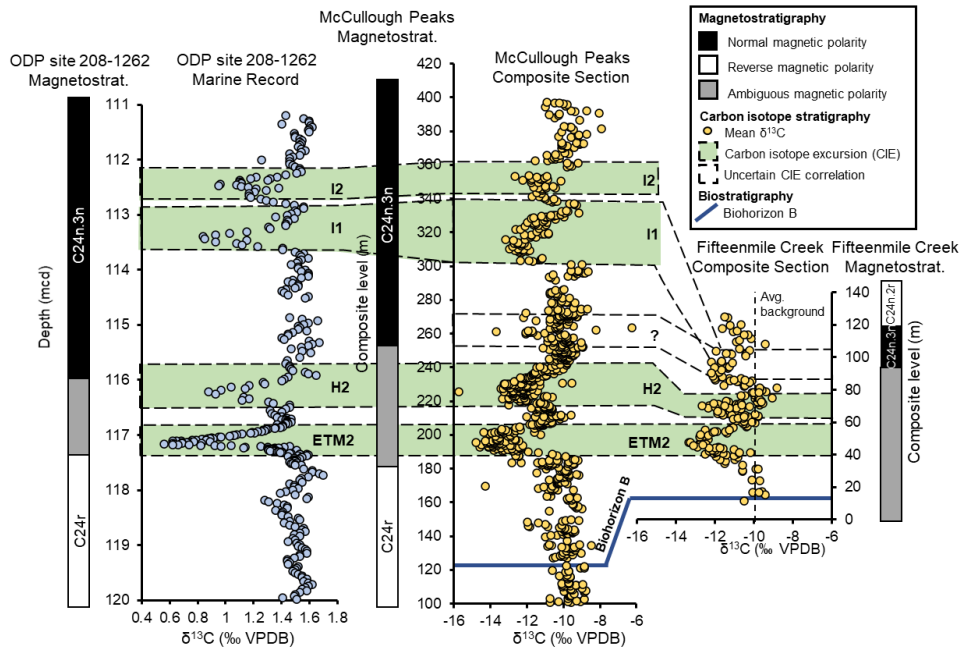


**Figure 6: Correlation between ODP site 208-1262 (from Zachos et al., 2010), McCullough Peaks (from Abels et al., 2016) and Fifteenmile Creek (this study). All points represent mean $\delta^{13}C$ values from a stratigraphic level. McCullough Peaks and Fifteenmile Creek records are shown at the same vertical scale. Two alternative correlations for the 85 – 104 m Fifteenmile Creek composite level interval are shown. Blue line shows the approximate level of Biohorizon B in both terrestrial locations. McCullough Peaks magnetostratigraphy from Clyde et al. (2007), Abels et al. (2012), and D'Ambrosia et al. (2017). Fifteenmile Creek magnetostratigraphy from Clyde et al. (2007) (measured at Elk Creek Rim) and Tauxe et al. (1994).**



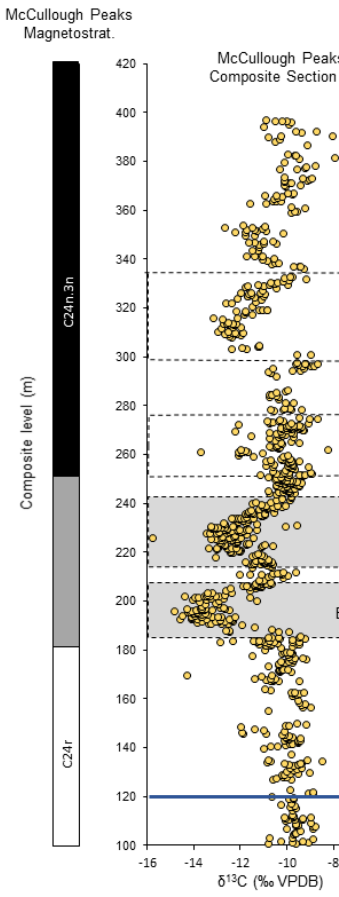


Deleted:

Deleted: 5

Deleted: Both

Deleted: The ETM2 and H2 hyperthermals are shaded in g and t

### 5.4 Correlation to mammal faunal events

The placement of the ETM2 and H2 CIEs in our new sections aligns with the levels predicted by Chew (2015) based on the levels of the B-1 and B-2 faunal events (Fig. 4). Error in the stratigraphic correlations used to construct the BCM framework or averaging of specific collecting levels within localities could both contribute to the small offsets between the CIE levels and the BCM levels that Chew (2015) predicted. Many of these localities have a relatively small number of specimens and would therefore have little effect on the faunal analysis (e.g., D–1403 has 34 specimens). The misplacement of richer localities, like D–1454 (1151 specimens) and D–1460 (405 specimens), would be more significant. These inconsistencies have likely muted the turnover signal observed by Chew (2015). Moreover, a confounding problem with correlating faunal turnover to many of these localities, is that fossiliferous horizons often occur at multiple levels within a locality. For example, in locality D–1350, mammal fossils have been collected both above and below the onset of the ETM2 excursion and most collection records are not precise enough to indicate which specimens came from which levels. Thus, a turnover signal could be muted by mixing taxa from within the excursion with pre- and post-excursion taxa. This problem can be overcome only by recollecting such localities using even higher stratigraphic precision.

More importantly, these results demonstrate that there is a reasonably large miscorrelation in the BCM levels of the localities south of Fifteenmile Creek, in the Basin Draw section, compared with north of the creek. South of Fifteenmile Creek, the BCM levels alone are not an accurate predictor of a locality's position relative to the hyperthermals. For example, the D–1454 and D–1460 localities (409 BCM level) are not within a CIE, despite this BCM level occurring within faunal event B–1 and overlapping with ETM2 in other sections (e.g., Basal/D–1350). We sampled a smaller isotope section directly through the D–1454 locality to test whether incorrect correlation to the main section could have contributed to this offset or in fact it falls within a CIE. The $\delta^{13}C$ record through the locality is consistent with that from the main section and suggests that it is not within ETM2 (Appendix B). It seems likely that the Basin Draw section localities should be shifted downwards by ~20 meters in the Bown et al. (1994) composite section. This would place the productive localities D–1454 and D–1460 within Biohorizon B and would likely strengthen the distinction between Biohorizon B and the subsequent faunal events B–1 and B–2 in a revised faunal analysis should further stratigraphic work demonstrate that this move is warranted.

The isotope results presented here suggest that correlation of key localities should be tested by constructing new locality-specific isotope records that can be directly tied to the mammal collection from the same locality, similar to the sections through D–1454, D–1207, and D–1532 (Appendix B). For example, the locality-specific isotope record for locality D–1207 (448 BCM level) shows that this locality records the onset of the H2 CIE, rather than its recovery, as predicted by the BCM levels. Developing similar sections through other individual localities, where the primary fossil producing layer can be reliably constrained and tied into a local dGPS elevation and stable isotope record and then compared to other localities either within or outside of CIEs, would clarify observed faunal turnover and its potential relationship to climate fluctuations. Such precise correlations could also be used to investigate other stratigraphic levels where we find CIEs, such as the 486 m BCM level, to see whether there is associated faunal change.

**Formatted:** Outline numbered + Level: 2 + Numbering St 1, 2, 3, … + Start at: 1 + Alignment: Left + Aligned at: 0" Indent at: 0.25"

**Moved up [1]:** Chew (2015) proposed that the 405–417 and 4 448 BCM levels could correspond to the ETM2 and H2 hyperthermals, based on the observed changes in mammal divers and rate of turnover in these intervals. The new Fifteenmile Cree isotope records presented here broadly support this hypothesis, w the ETM2 hyperthermal overlapping with the 405–417 m interva (faunal event B–1) and H2 overlapping with the 435–448 m inter (faunal event B–2) (Figs. 4 and 6). This is especially apparent in Basal/D–1350, Kraus Flats, and North Fork sections north of Fifteenmile Creek. The D–1350 locality (408–410 BCM level), f example, shows a clear CIE consistent with ETM2 and also yield several species that first appear during faunal event B–1 (e.g., *Xenicohippus grangeri*, *Diacodexis secans*, *Didymictis lysitensis* *Eohippus angustidens*). Localities D–1410 (410–418 BCM level and D–1204 (438–444 BCM level), which we tied into the Kraus Flats section, produce faunas that are consistent with B–1 (D–14 and B–2 (D–1204), and also overlap with the ETM2 and H2 intervals, respectively. However, some localities show small offs from their predicted position relative to the CIE record. Locality 1311 (442 BCM level), for example, falls within the interval associated with faunal event B–2, but is just above the CIE associated with H2. Locality D–1403 (420 BCM level) is within ETM2 CIE but fell outside of the interval reported to contain fau event B–1 (Fig. 6).

**Deleted:** these

**Deleted:** the BCM level of locality D–1459 (438 m) suggests t it should fall within H2. The stable isotope record from the Basin Draw section, together with dGPS elevations, suggest this localit instead within ETM2 (Figs. 4 and 6). Additionally,

**Deleted:** A

**Deleted:** A

**Deleted:** end as implied by the stratigraphic range reported for faunal event B–2

**Formatted:** Not Highlight

**Deleted:** the apparent lack of faunal change near the 486 m BC level (Chew, 2015), where we do find a small negative CIE (Fig.

## 6 Conclusions

The ETM2, H2 and potentially I1 hyperthermals are recognized for the first time in pedogenic carbonate from the south-central Bighorn Basin (Fifteenmile Creek area). Correlation of the ETM2 and H2 carbon excursions with the faunal record, supports previous suggestions that some mammalian turnover in the early Wasatchian North American Land Mammal Age, following the PETM, is associated with early Eocene hyperthermals. The new isotope records presented here also highlight some of the complexities of lithological correlation between the low-lying exposures in Fifteenmile Creek area and support the use of an independent means of stratigraphic correlation, such as precise elevation, in conjunction with mammalian biostratigraphy and carbon isotope chemostratigraphy. The magnitudes of the ETM2 and H2 CIEs (3.1 ‰ and 1.7 ‰, respectively) are smaller than what is seen farther north in the McCullough Peaks region of the Bighorn Basin (3.8 ‰ and 2.8 ‰). We suggest that local variation in water availability to plants, and potentially other vegetation and soil processes, likely account for much of the differences in carbon isotope values observed between the two locations.

## Appendix A

To sample in the relatively low relief terrain of the Fifteenmile Creek area, the six main sections were measured as a series of subsections (Figs. A1 – A6). Subsections were measured using a Jacob's staff and tied together using either bed traces or correlation by siting a horizontal line (Fig. A7). Differential GPS elevations were measured from each section to place the carbon isotope results into an elevation framework and fossil localities were either sampled directly or traced into the sections to allow the isotope data to be placed into the composite stratigraphy of Bown et al. (1994) (Fig. A8). Meter levels within an individual subsection and bed traces over short distances have less than 1 m of uncertainty, typical for measurements using a Jacob's staff and clinometer. In places, sections were correlated to one another using bed traces and other correlations between sections used BCM levels of fossil localities that were measured in (Fig. A9). Bed traces over longer distances between sections may have an uncertainty of up to ~10 meters.

Sampling was done over four years (2015 – 2018) and differential GPS elevation measurements were taken during the final year of field work (2018). Differential GPS points were preferentially taken at levels that correspond to isotope excursions and secondarily at the base and top of each subsection. In places where the base/top of a subsection was uncertain at the time of dGPS measurements, a sample site was selected that could be confidently located to help constrain the subsection. Carbon isotope results for each section shown according to subsection is included in Fig. A10.

**Basin Draw:** The Basin Draw section is made up of 7 subsections and includes ~60 total meters of section (Fig. A1). Bed tracing over a long distance was facilitated by the presence of a distinct red – purple – white "barren marker bed". Three fossil localities (D-1458, D1454, D-1460) were correlated to the section via bed traces and a fourth locality (D-1459) was sampled

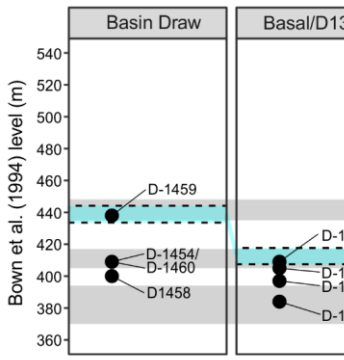


**Deleted:**

**Deleted:** <#>**Figure 6: Selected Fifteenmile Creek fossil localities tied to the Bown et al. (1994) composite section. Shading follows Fig. 4, where stratigraphically lowest, midd and highest carbon isotope excursions are outlined by blue, yellow and red shading, respectively. The stratigraphic intervals associated with the faunal events described in Che (2015) are shown as grey shaded regions. Points for the foss localities incorporate some stratigraphic uncertainty and averaging of collecting levels discussed in the text. For more detailed ranges of collecting levels associated with the locali see Fig. 3.¶**

**Effects of landscape heterogeneity on terrestrial carbon isot records¶**

The degree of isotopic fractionation in terrestrial systems can va depending on environmental factors, many of which are known fluctuate during hyperthermals. Together, these factors can complicate efforts to use paleosol carbonate $\delta^{13}C$ to reconstruct atmospheric $\delta^{13}C$ fluctuations, which is critical for understandin the source of carbon input during hyperthermals as well as understanding how these changes could be recorded differently across a landscape. These fractionation steps can be broadly grouped into those associated with local vegetation (e.g., fractionation associated with photosynthesis and respiration) an those related to soil processes (e.g., microbial respiration, diffus through soil, and calcite precipitation) (Koch, 1998). ¶

Carbon isotope fractionation in plants is dependent on light, wa availability, temperature, soil nutrients, and atmospheric *p*CO2 (e.g., O'Leary, 1988; Farquhar et al., 1989). The strongest singl environmental control on $\delta^{13}C$ values in C3 vegetation is water availability to plants, which accounts for about half of the variability, with plants discriminating less against $^{13}C$ during dr times (Ehleringer, 1993; Stewart et al., 1995; Diefendorf et al., 2010; Kohn, 2010, 2016). Position on the landscape can also af water stress on vegetation by affecting soil drainage. Thus,

**Deleted:** southern

**Deleted:** 2.4

**Deleted:** 3

directly for isotope samples. Locality D-1454 was also sampled independently as a shorter section (Appendix B). Subsection 6 includes the fossil locality D-1459 (438 m BCM level) and appears to be part of a cut-and-fill sequence, introducing some additional uncertainty into the upper part of this section. It was not possible to trace beds between the Basin Draw section and other sections in this study due to the intervening 15-mile Creek. Correlation between Basin Draw and the other sections therefore relies on the stratigraphic level of the fossil localities which can be supplemented with dGPS elevations and chemostratigraphic patterns.

**Basal/D-1350:** The Basal/D-1350 section includes 6 subsections and includes ~52 total meters of section (Fig. A2). In places, individual samples were collected along a bed trace and were not part of a separate subsection (e.g., between subsections 1 and 2 and between subsections 4 and 5). Correlation between subsections 2 and 3 and between subsections 3 and 4 were done by siting a horizontal line between exposures and these correlations have an uncertainty of ± 1.5 m and ±5 m, respectively. Fossil localities D-1370 and D-1758 were correlated into the section via bed traces and localities D-1350 and D-1538 were sampled directly. Rough bed tracing was done between the top of this section to the base of the North Fork section, however lining up minimum CIE values for each section offers the most reliable means of correlating the two sections. The 409 BCM level at the D-1350 locality can also be used to correlate to the 409 BCM level D-1454 and D-1460 localities in the Basin Draw section.

**Kraus Flats:** The Kraus Flats section was measured as a parallel section to North Fork to capture the middle two CIEs. This sections also allowed the productive fossil locality D-1204 ("Kraus Flats") to be tied into the isotope framework. It includes 5 subsections and ~ 55 total meters of section (Fig. A3). Fossil locality D-1410 was sampled directly through two distinct fossil producing levels (D-1410 mid and D-1410 top). D-1410 mid also preserves the H2 CIE in a yellow-grey mottled paleosol (Fig. A8). Localities D-1822 and D-1204 were correlated to the section via bed traces. A distinct purple marker bed ("Kraus Flats purple marker") facilitated correlation for the top of the section, moving up towards locality D-1204. No beds were traced between Kraus Flats and the other sections. Correlating minimum CIE values is the preferred method for tying Kraus Flats to the other sections.

**North Fork:** The North Fork section includes 8 subsections and ~35 total meters of section (Fig. A4). Two distinct and relatively continuous purple marker beds ("Purple #1" and "Purple #2") facilitated correlation between several short subsections. Subsections 4 and 5 were sampled at a later date to fill in sampling gaps around potential CIE levels. These subsections were tied into the existing North Fork framework by measuring up to existing sample sites that could be confidently located (CBH15-SN32 and CBH15-SN33). Fossil locality D-1403 was correlated to subsection 1 via bed trace and fossil localities D-1295 and D-1311 were sampled directly. A purple bed near the top of subsection 6 was traced to the base of the Upper North Fork section. The long distance of this trace, combined with evidence from dGPS elevations and BCM levels for the two sections suggest an uncertainty of ~ 10 m on this correlation.

**Upper North Fork:** The Upper North Fork section includes 3 subsections and ~28 total meters of section (Fig. A5). The highest CIE (I1?) is preserved in a yellow-grey paleosol, just above a thin, discontinuous grey sandstone (Fig. A8). Fossil locality D-1257 was correlated to subsection 3 in this section via bed trace. The base of a purple bed in a red-purple couplet

was traced between subsections 1 and 2 and also between subsection 2 and the base of our Red Butte section. This bed trace has ~ XX m of uncertainty, due to the long distance.

**Red Butte:** The Red Butte section includes 3 subsections and ~48 total meters of section (Fig. A6). The purple bed near the base of subsection 1 was traced from the Upper North Fork section. Isotope samples near the base of subsection 1 were collected just above fossil locality D-1491. Fossil locality D-1532 is located near the Red Butte section and was also correlated to the red-purple couplet at the base of this section as well. D-1532 was also sampled independently as one of the short fossil locality isotope sections (Appendix B).

Formatted: Font: Bold

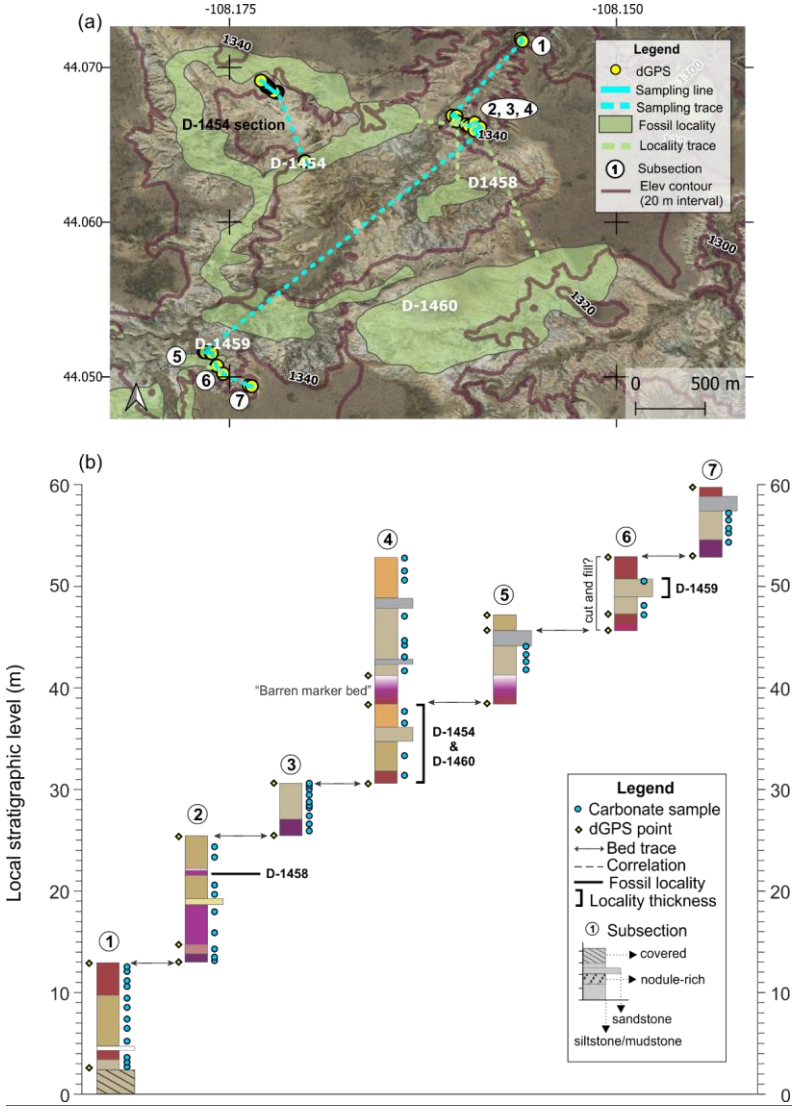


**Figure A1: Basin Draw section (a) map and (b) diagram showing sampling subsections, dGPS tie points, bed traces, and correlated fossil localities. Colored boxes in (b) represent the surface color of weathered rocks.**

Formatted: Keep with next

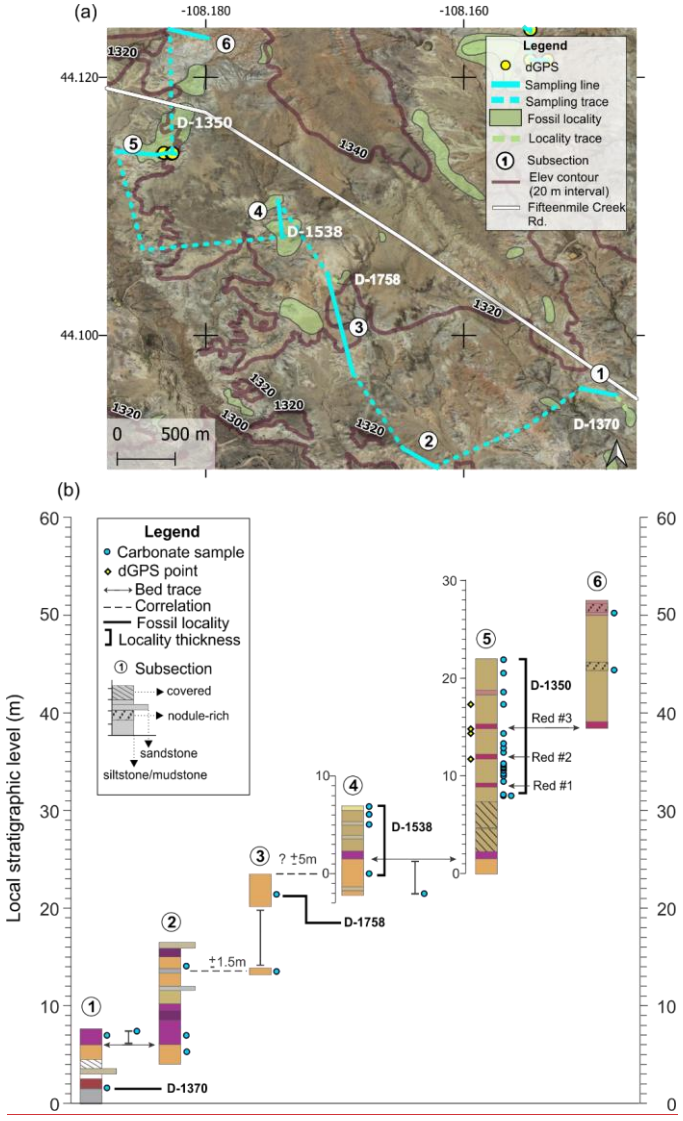


995 **Figure A2: Basal/D-1350 section (a) map and (b) diagram showing sampling subsections, dGPS tie points, bed traces, and correlated fossil localities. Colored boxes in (b) represent the surface color of weathered rocks.**

Formatted: Keep with next

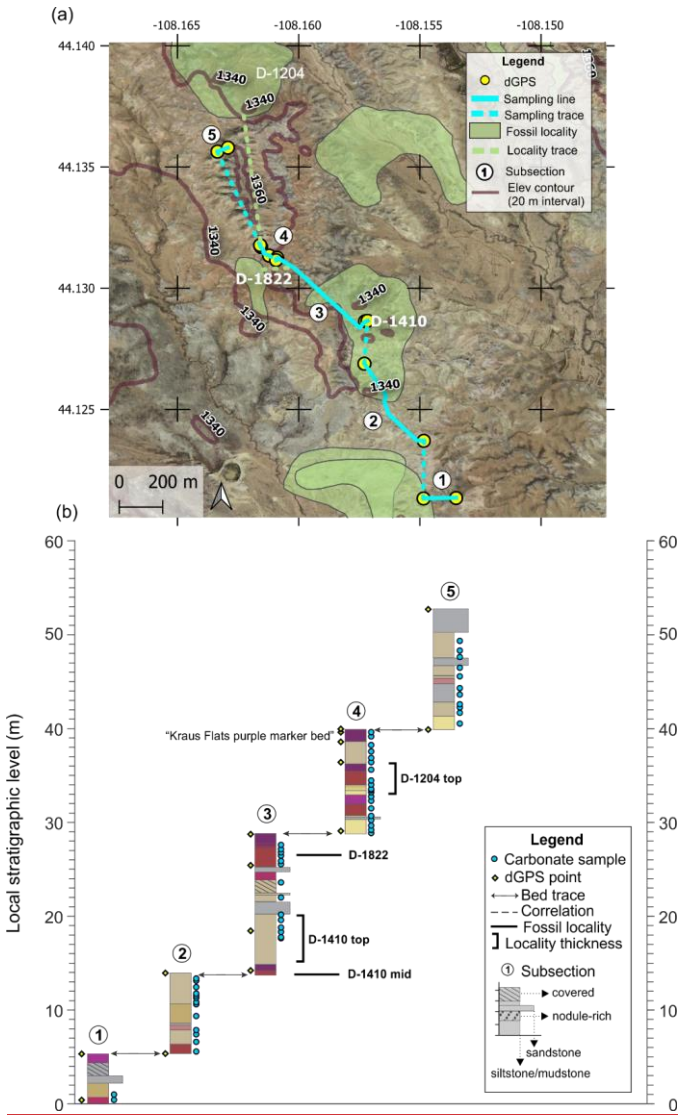


**Figure A3: Kraus Flats section (a) map and (b) diagram showing sampling subsections, dGPS tie points, bed traces, and correlated fossil localities. Colored boxes in (b) represent the surface color of weathered rocks.**

Formatted: Keep with next

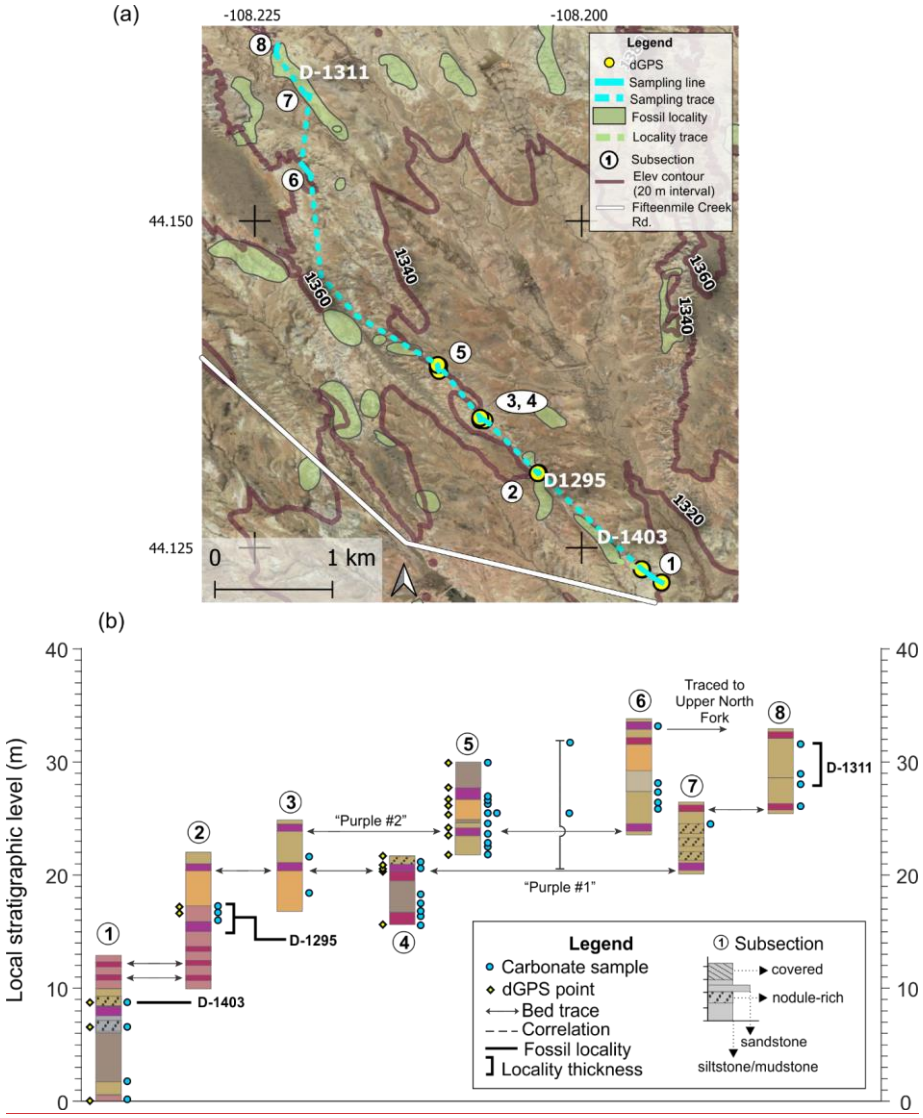


**Figure A4: North Fork section (a) map and (b) diagram showing sampling subsections, dGPS tie points, bed traces, and correlated fossil localities. Colored boxes in (b) represent the surface color of weathered rocks.**



**Formatted:** Keep with next

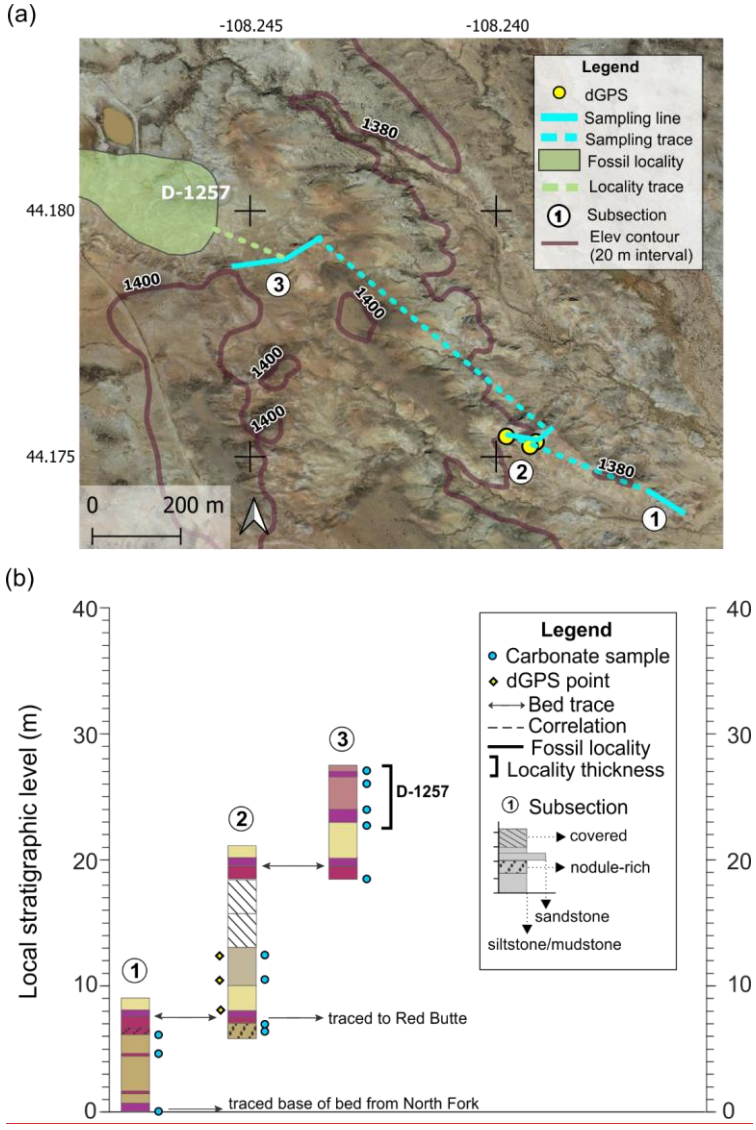


**Figure A5: Upper North Fork section (a) map and (b) diagram showing sampling subsections, dGPS tie points, bed traces, and correlated fossil localities. Colored boxes in (b) represent the surface color of weathered rocks.**



Formatted: Keep with next

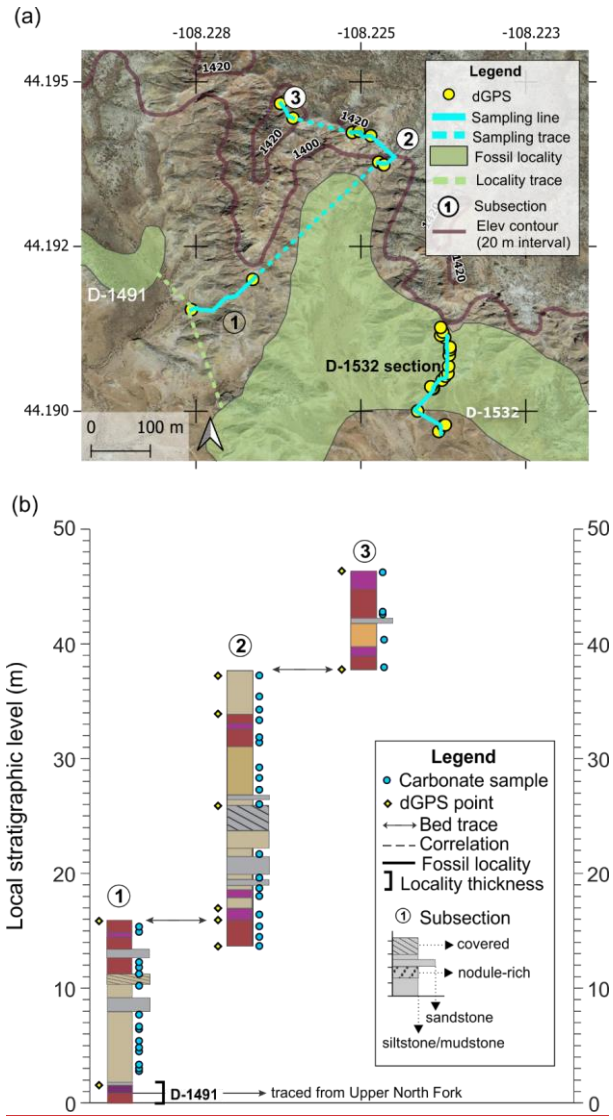


**Figure A6: Red Butte section (a) map and (b) diagram showing sampling subsections, dGPS tie points, bed traces, and correlated fossil localities. Colored boxes in (b) represent the surface color of weathered rocks.**



**Formatted:** Keep with next

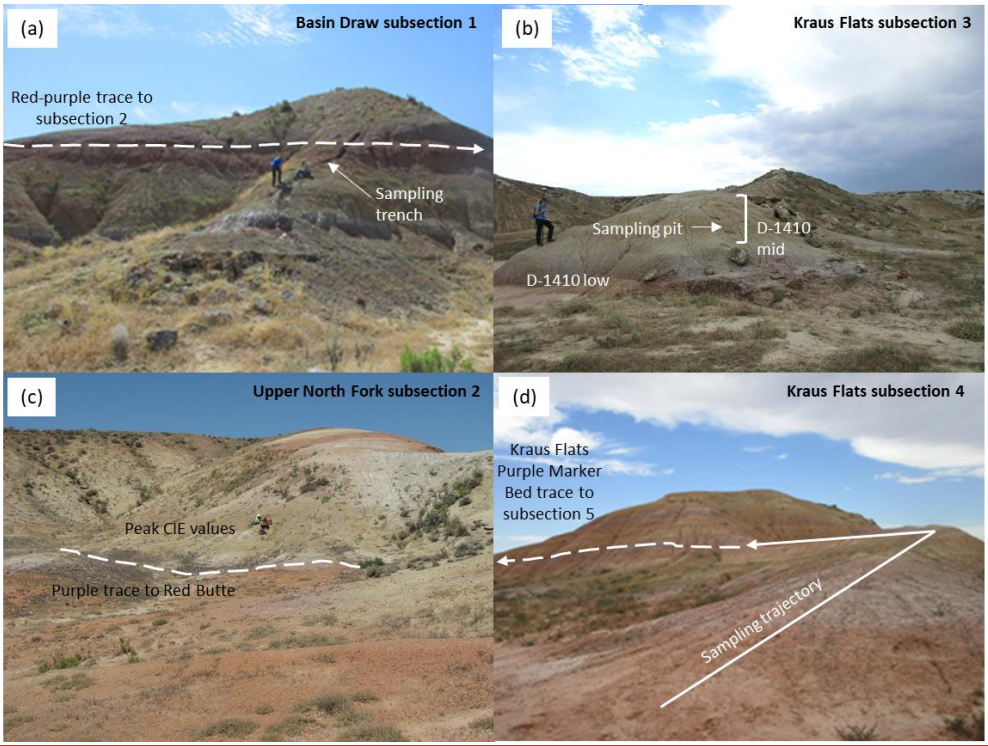


Figure A7: Field photos of representative sections. (a) Basin Draw subsection 1, showing sampling trench and red-purple contact traced to subsection 2. (b) Kraus Flats Subsection 3, showing fossil locality D-1410 collecting levels and carbonate sampling pits. Yellow bed with sample pits represents middle collecting level in D-1410 locality and ETM2 excursion. (c) Upper North Fork subsection 2, showing red-purple contact traced to Red Butte section and peak "I1" excursion in the yellow paleosol. (d) Kraus Flats subsection 4, showing sampling trajectory through H2 excursion and Kraus Flats Purple Marker Bed traced to subsection 5. Person for scale in a – c.

Formatted: Keep with next

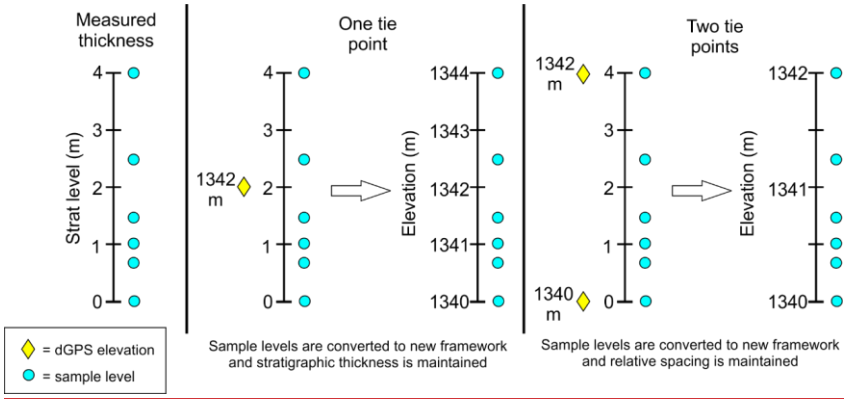


**Figure A8: Conversion between measured stratigraphic thickness to elevation using one or two tie points. The same method was used for converting to BCM levels using correlated fossil localities as tie points.**

Formatted: Centered, Keep with next

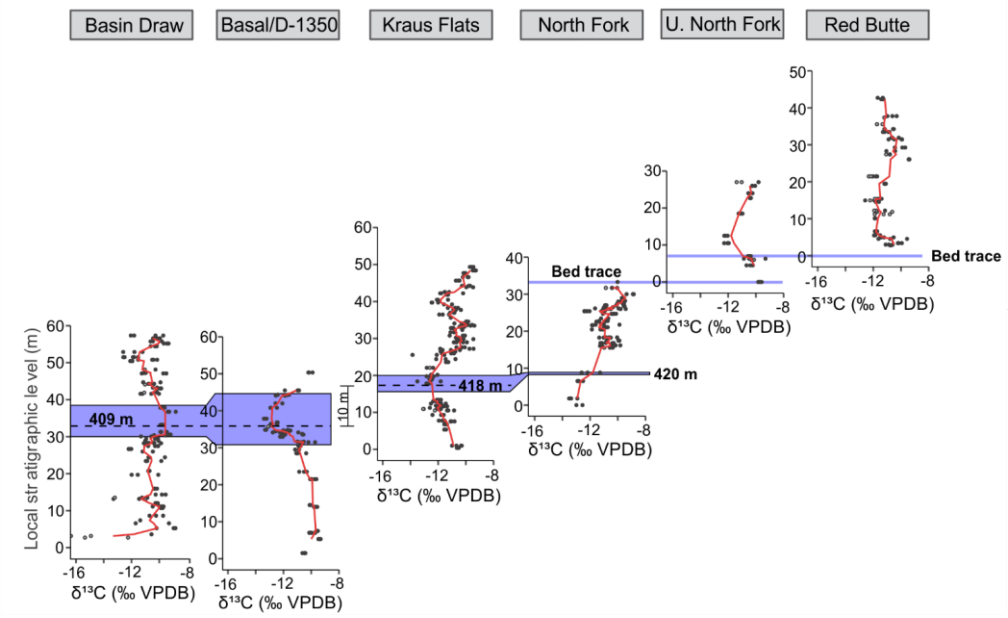


**Figure A9: Section correlations based on bed traces and fossil locality levels. Stratigraphic levels represent meter levels measured using a Jacob's staff. Bed traces are used to correlate between the North Fork and Upper North Fork sections and between the Upper North Fork and Red Butte sections. Fossil localities that occur at the 409 BCM level in the Basin Draw and Basal/D-1350 sections are used to correlate these sections. Fossil localities that occur near the 420 BCM level in the Kraus Flats and North Fork sections are used to correlate these sections and the difference between these BCM levels helps tie the Basin Draw, Basal/D-1350, and Kraus Flats sections together. This correlation is also supported by bed traces between the Basal/D-1350 and North Fork sections.**

Formatted: Keep with next

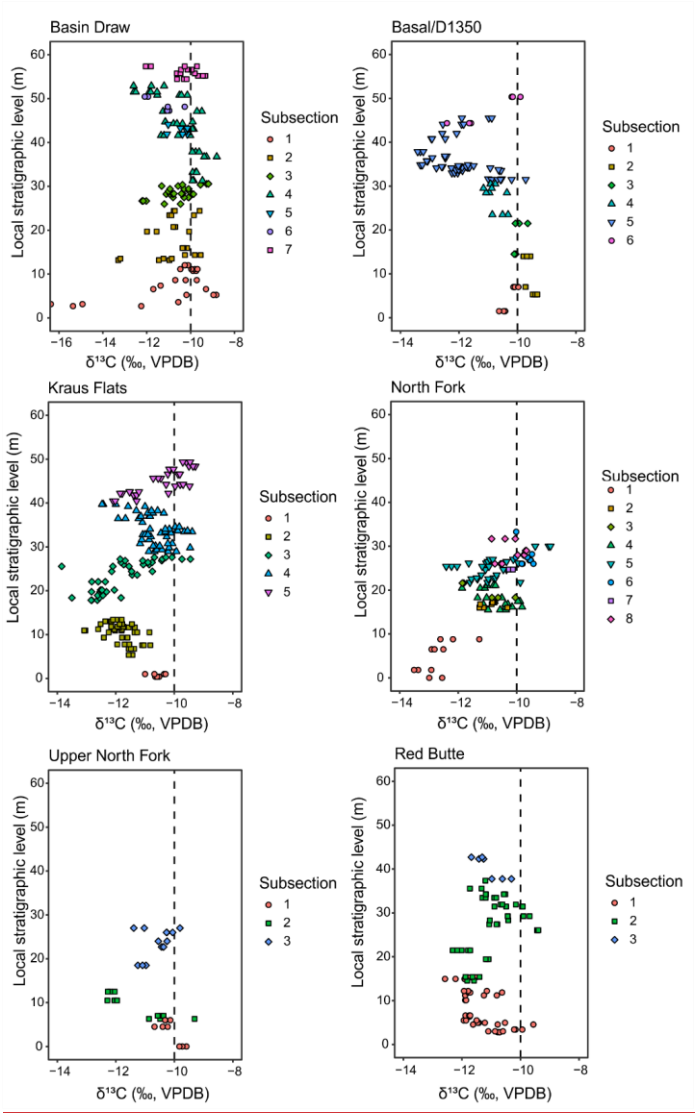


**Figure A10: Carbon isotope stratigraphy for each section with symbols showing different subsections. Points represent individual sample measurements. Black dashed line at -10 ‰ shows typical background value for Fifteenmile Creek.**

Formatted: Keep with next

Formatted: Caption

**Appendix B**

**Carbon isotopes stratigraphy through fossil localities**

Three locality-specific stratigraphic sections were collected for stable isotope analysis to identify whether they captured a CIE. If a CIE fell entirely within the fossil producing levels of a single locality, future fossil collecting could target these areas for more refined faunal analyses that would eliminate uncertainty related to stratigraphic averaging and correlation between sections. The three localities: D–1454 (409 BCM), D–1207 (448 BCM), and D–1532 (485 BCM) were selected because they are found at important levels associated faunal events B–1 (D–1454) or B–2 (D–1207) or near an unresolved CIE (D–1532). These smaller locality-specific sections can then be compared to their nearest main section using the BCM levels and elevation to further assess spatial variability in $\delta^{13}C$ and confirm the correlations (Fig. B1). The carbon isotope values are relatively consistent over short distances in Fifteenmile Creek (Fig. B1). The Bown et al (1994) composite level (BCM) and dGPS elevation are also both fairly reliable stratigraphic indicators over short traces and correlate the locality sections to the main sections in consistent ways (Fig. B1). An exception to this is correlating the D–1207 locality to the Kraus Flats section, where the BCM level lines up with the H2 excursion, but the dGPS elevations have them offset from each other. D–1207 (448 BCM level) is the only one of these three localities that falls within an excursion (H2). This level is predicted to be within the B–2 faunal event in Chew (2015) (435 to 448 m). D–1207 has two taxa that first appear in faunal event B–2 (*Hexacodus sp*. and *Protorohippus venticolum*), and this locality therefore represents a place where the carbon isotope stratigraphy and biostratigraphy are consistent and suggest that it falls within H2 and the B–2 faunal event. It also illustrates a need to use both BCM and dGPS for precise correlation of carbon isotope stratigraphy in this area.

Deleted: A

Deleted: A

Deleted: A

Deleted: A

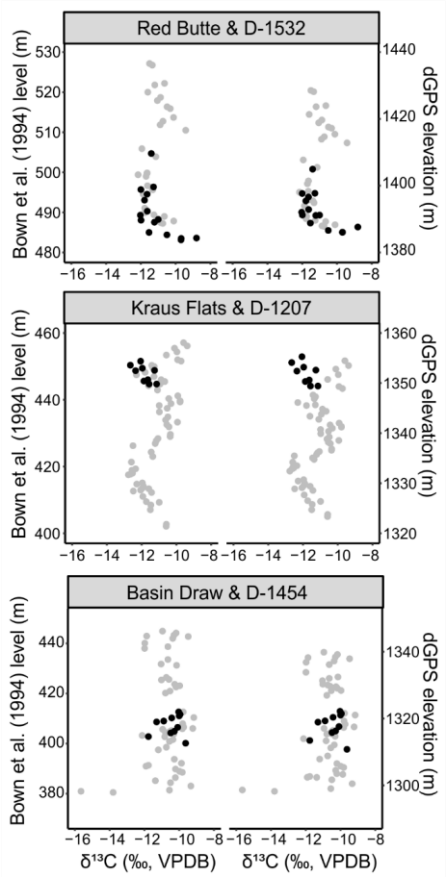


**Figure B1: Carbon isotope stratigraphy through the (a) D–1532 (485 BCM level), (b) D–1207 (448 BCM level), and (c) D–1454 (409 BCM level) fossil localities (black) along with the nearest main section (grey). Points represent average $\delta^{13}C$ from a stratigraphic level. All data are shown according to their Bown et al. (1994) equivalent meter level (left) and differential GPS elevation (right).**

Deleted: A

## Appendix C

Deleted: B

### Inter-laboratory offsets and correction

Comparison of the carbon and oxygen isotope data from samples run at both CUBES–SIL and UMSIL shows that CUBES–SIL produces generally lower values than UMSIL in this dataset's range of values. This offset to lower values is systematic

and is larger at progressively lower values. This issue affects both isotopes but is particularly true for carbon, which suggests that subtle differences in instrumentation and standardization procedure are the causes of this offset. UMSIL uses a ThermoFisher MAT253 attached to a Kiel IV automated preparation device and data are normalized using a best-fit linear regression to NBS-18 and NBS-19 reference materials ($\delta^{13}C$ = -5.01 ‰ and +1.95 ‰, $\delta^{18}O$ = -23.2 ‰ and -2.20 ‰, respectively) by regressing measured, $^{17}O$-corrected values against the published values for the standards. Corrections are determined for both carbon and oxygen and these corrections are checked routinely using either NBS-18, NBS-19, or both, and tend to be stable over several months.

CUBES–SIL uses a Thermo Delta V gas source, continuous flow isotope ratio mass spectrometer. Samples are measured along with 3–4 standards that either have internationally accepted values or are in-house standards that have values determined relative to these standards (e.g., NBS-18, NBS-19, and LVSEC for light $^{13}C$ standards). Measurements of the standards bracket sample measurements in each run and are used to assess behaviors of the instrument that may need to be corrected. Standards covering the full range of signal intensities observed in the samples are measured to assess effects of linearity. Standards are also run intermittently throughout the analytical session to evaluate instrument drift over the course of a run. Lastly, the overall offset of the standards from accepted values is evaluated. These corrections are done independently for carbon and oxygen and are checked using a monitoring standard that is treated as an unknown. In this dataset, linearity and drift were often negligible, and corrections for these effects were only applied when needed. Raw or linearity/drift corrected values were then corrected to final values similarly to UMSIL, by applying a regression between two standards that span a range in values. Runs 1–13 and 15 used NBS-18 as the negative anchor for both $\delta^{13}C$ and $\delta^{18}O$, while runs 14, 16, and 17 used a MERCK carbonate as the negative $\delta^{13}C$ anchor point ($\delta^{13}C$ = -35.6 ‰), to better standardize for the range of $\delta^{13}C$ values found in typical terrestrial carbonates, following recommendations in Coplen et al. (2006).

Both UMSIL and CUBES–SIL used NBS-18 as the negative $\delta^{13}C$ for most measurements. NBS-18 is ~4–10 ‰ higher than most of the measurements in this dataset, so the linear regression that is used for the scale correction in both labs is extrapolated far beyond that lowest anchor point. As a result, uncertainties in this regression in both labs, while small, can result in differences in sample values that are larger than analytical uncertainty. If this were the cause of the difference in sample values between CUBES–SIL and UMSIL, one would expect to see correlation between the values from both labs, as well as a progressively larger offset between sample values at more negative $\delta^{13}C$ values. A strong correlation and positive slope are seen between the isotope ratios measured at CUBES–SIL relative to UMSIL in both $\delta^{13}C$ and $\delta^{18}O$ values for a small subset of samples that were run in both labs (Fig. C1). The strength of the correlation for $\delta^{13}C$ suggests that we can correct data run from one lab to be on scale with the other lab ($R^2$ = 0.88, S = 0.37 ‰). We compared a subset of values produced at CUBES–SIL using either NBS-18 or the lower MERCK standard for the same sample. This showed no systematic difference in the values (Fig. C2), which suggests that CUBES–SIL data are internally consistent, despite the extrapolation of the scale correction for many of the runs. Given that, and that the majority of this dataset was analyzed at CUBES–SIL, we have chosen to correct the UMSIL data to these values, using the regression equations for both carbon and oxygen (Fig. C1). After applying the correction, the UMSIL data become more negative, while still following the same stratigraphic patterns in $\delta^{13}C$ (Fig. C3).

Deleted: B

Deleted: B

Deleted: B

Deleted: B

While we think that this correction scheme is most appropriate for these data, we recognize that it may complicate comparisons to other previously published work that do not use $\delta^{13}C$ standards that account for values in this range. Further, because the $\delta^{13}C$ correlation between labs is strong, the magnitudes of the CIE's are not appreciably affected in the combined data after correction. Oxygen isotope values exhibit a weaker correlation between the labs ($R^2 = 0.74$), indicating that considerably more noise is added by combining the data. However, highly precise $\delta^{18}O$ values are not important for our interpretations.

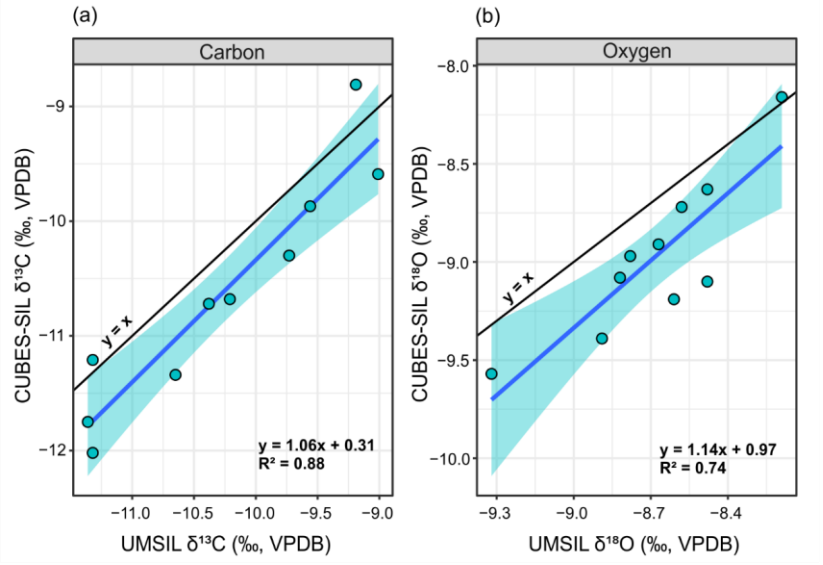


**Figure C1: Ten replicate samples analyzed at the University of Colorado Boulder (CUBES–SIL) and University of Michigan (UMSIL), shown according to their $\delta^{13}C$ (a) and $\delta^{18}O$ (b). Black lines indicate a 1:1 relationship between the two labs and blue lines with shading represent the regressions between the two labs that were used to correct the data.**

Deleted: B

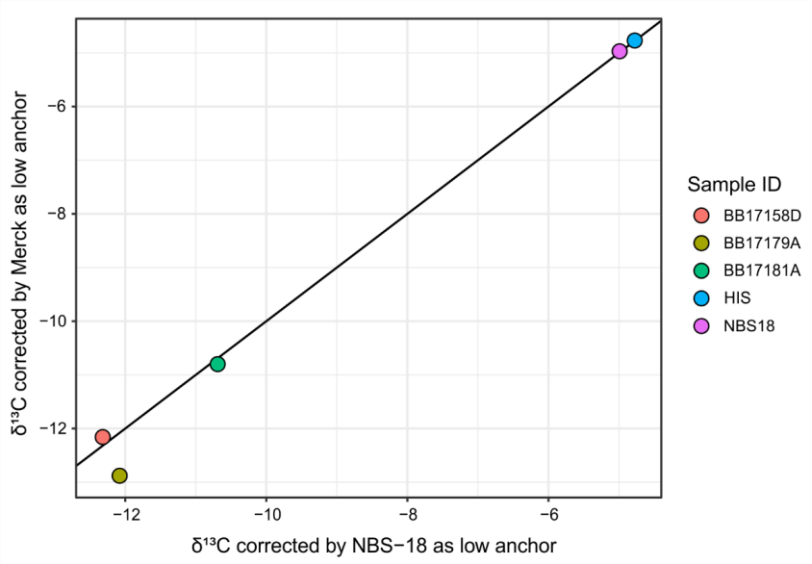


**Figure C2: $\delta^{13}C$ values for standards and a subset of samples that were run in a session that used NBS-18 as a low $\delta^{13}C$ anchor, as well as in a session that used MERCK as the low $\delta^{13}C$ anchor. Most fall on the 1:1 line (black line), and the two samples that fall off the line show no systematic offset suggesting the difference in those values is not due to the difference in anchor standard.**

Deleted: B

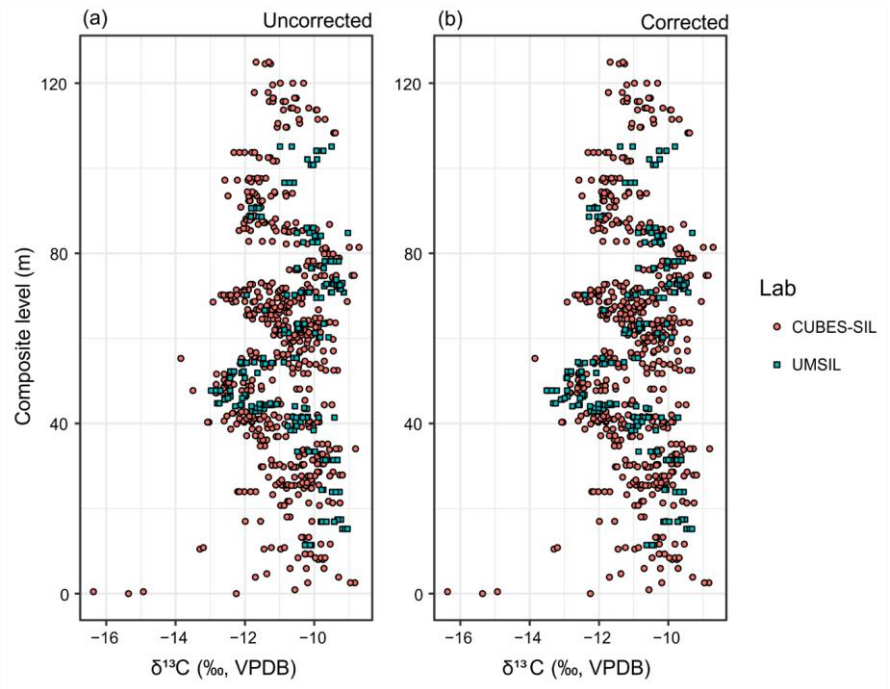


**Figure C3: Pedogenic carbonate $\delta^{13}C$ showing samples that were analyzed in the UMSIL lab uncorrected (a) and corrected (b), using the carbon regression equation from Fig. B2. Points represent individual sample measurements. The corrected UMSIL values (b) are used throughout the text. This composite section includes the Basin Draw and D-1454 sections with the top of the Basin Draw section correlated to the lowest CIE (ETM2).**

Deleted: B

## Appendix D

Deleted: C

### Oxygen Isotopes

A seven-point moving average through all samples in the composite section do not show clear excursions in the oxygen isotope record (Fig. D1). Moreover, there is no discernible difference between excursion and non-excursion $\delta^{18}O$ values when these intervals are binned together and averaged (see supplemental data).

Deleted: C

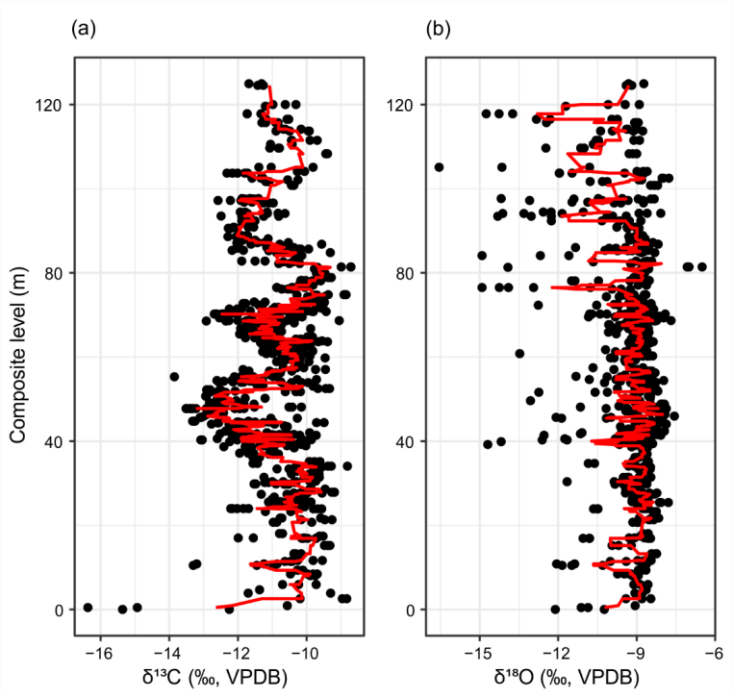


**Figure D1: Pedogenic carbonate $\delta^{13}C$ (a) and $\delta^{18}O$ (b) according to their composite stratigraphic level. Points represent individual sample measurements. Red line is a seven-point moving average through the values. This composite section includes the Basin Draw and D-1454 sections with the top of the Basin Draw section correlated to the lowest CIE (ETM2).**

Deleted: C

## Data availability

Raw and processed stable isotope data, as well as R scripts used for data processing and creating figures are available in Open Science Framework (OSF) and can be accessed here: https://osf.io/3z2xc/?view_only=1e9f419b168c43f5b0ae0b8e8f09584a

## Author contribution

W.C.C., R.S., and A.E.C. acquired the initial funding. S.J.W., W.C.C., R.S., and A.E.C., were involved in project conceptualization and fieldwork. S.J.W., R.S., and K.E.S. contributed to laboratory investigation and analyses. All authors contributed to writing and editing of the manuscript.

## Competing Interests

The authors declare that they have no conflict of interest.

## Acknowledgements

This project was supported by National Geographic Grant # 9969-16 and a University of New Hampshire Natural Resources and Earth Systems Science Graduate Student Research Grant. We also thank L. Wingate and the UMSIL laboratory as well as B. Davidheiser-Kroll of the CUBES–SIL laboratory for stable isotope analyses, S. Kopf for development and implementation of IsoVerse R package used in the data reduction methods developed by CUBES–SIL, K. Rose, D. Todd, D. Hock, R. Gillham for field assistance, and M. Routhier for the differential GPS equipment and post-processing. We are also grateful to the Bureau of Land Management and Brent Breithaupt for providing a Paleontological Resources Use Permit to A.E.C.. We thank C. Bataille, G. Bowen, and H. Abels for their helpful comments on an earlier draft of this work. Field work for this study was conducted on the ancestral and traditional lands of the Cheyenne, Crow, and Oceti Sakowin (Sioux), Eastern Shoshone, and Northern Arapahoe Indigenous peoples along with other Native tribes who call the Bighorn Basin and Rocky Mountain region home. We acknowledge and honor with gratitude the land and people who have stewarded it for generations.

## References

Abels, H. A., Clyde, W. C., Gingerich, P. D., Hilgen, F. J., Fricke, H. C., Bowen, G. J., and Lourens, L. J.: Terrestrial carbon isotope excursions and biotic change during Palaeogene hyperthermals, 5, 326–329, https://doi.org/10.1038/ngeo1427, 2012.

Abels, H. A., Lauretano, V., van Yperen, A. E., Hopman, T., Zachos, J. C., Lourens, L. J., Gingerich, P. D., and Bowen, G. J.: Environmental impact and magnitude of paleosol carbonate carbon isotope excursions marking five early Eocene hyperthermals in the Bighorn Basin, Wyoming, 12, 1151–1163, https://doi.org/10.5194/cp-12-1151-2016, 2016.

Agnini, C., Fornaciari, E., Raffi, I., Rio, D., Röhl, U., and Westerhold, T.: High-resolution nannofossil biochronology of middle Paleocene to early Eocene at ODP Site 1262: implications for calcareous nannoplankton evolution, 64, 215–248, 2007.

Agnini, C., Macrì, P., Backman, J., Brinkhuis, H., Fornaciari, E., Giusberti, L., Luciani, V., Rio, D., Sluijs, A., and Speranza, F.: An early Eocene carbon cycle perturbation at ~52.5 Ma in the Southern Alps: chronology and biotic response, 24, PA2209. doi:10.1029/2008PA001649., 2009.

Agrawal, S., Verma, P., Rao, M. R., Garg, R., Kapur, V. V., and Bajpai, S.: Lignite deposits of the Kutch Basin, western India: Carbon isotopic and palynological signatures of the early Eocene hyperthermal event ETM2, Journal of Asian Earth Sciences, 146, 296–303, https://doi.org/10.1016/j.jseaes.2017.04.030, 2017.

Arreguin-Rodriguez, G. J. and Alegret, L.: Deep-sea benthic foraminiferal turnover across early Eocene hyperthermal events at Northeast Atlantic DSDP Site 550, 451, 62–72, http://dx.doi.org.libproxy.unh.edu/10.1016/j.palaeo.2016.03.010, 2016.

Aziz, H. A., Hilgen, F. J., van Luijk, G. M., Sluijs, A., Kraus, M. J., Pares, J. M., and Gingerich, P. D.: Astronomical climate control on paleosol stacking patterns in the upper Paleocene–lower Eocene Willwood Formation, Bighorn Basin, Wyoming, Geol, 36, 531, https://doi.org/10.1130/G24734A.1, 2008.

Baczynski, A. A., McInerney, F. A., Wing, S. L., Kraus, M. J., Bloch, J. I., Boyer, D. M., Secord, R., Morse, P. E., and Fricke, H. C.: Chemostratigraphic implications of spatial variation in the Paleocene-Eocene Thermal Maximum carbon isotope excursion, SE Bighorn Basin, Wyoming, Geochem. Geophys. Geosyst., 14, 4133–4152, https://doi.org/10.1002/ggge.20265, 2013.

Baczynski, A. A., McInerney, F. A., Wing, S. L., Kraus, M. J., Bloch, J. I., and Secord, R.: Constraining paleohydrologic change during the Paleocene-Eocene Thermal Maximum in the continental interior of North America, Palaeogeography, Palaeoclimatology, Palaeoecology, 465, 237–246, https://doi.org/10.1016/j.palaeo.2016.10.030, 2017.

Barnet, J. S. K., Littler, K., Westerhold, T., Kroon, D., Leng, M. J., Bailey, I., Röhl, U., and Zachos, J. C.: A high-fidelity benthic stable isotope record of Late Cretaceous–early Eocene climate change and carbon-cycling, Paleoceanography and Paleoclimatology, 34, 672–691, https://doi.org/10.1029/2019PA003556, 2019.

Bowen, G. J.: Up in smoke: A role for organic carbon feedbacks in Paleogene hyperthermals, Global and Planetary Change, 109, 18–29, https://doi.org/10.1016/j.gloplacha.2013.07.001, 2013.

Bowen, G. J. and Bowen, B. B.: Mechanisms of PETM global change constrained by a new record from central Utah, 36, 379–382, 2008.

Bowen, G. J., Koch, P. L., Gingerich, P. D., Norris, R. D., Bains, S., and Corfield, R. M.: Refined isotope stratigraphy across the continental Paleocene-Eocene boundary on Polecat Bench in the northern Bighorn Basin, 33, 73–88, 2001.

Bowen, G. J., Clyde, W. C., Koch, P. L., Ting, S., Alroy, J., Tsubamoto, T., Wang, Y., and Wang Y.: Mammalian dispersal at the Paleocene/Eocene boundary, 295, 2062–2065, 2002.

Bowen, G. J., Beerling, D. J., Koch, P. L., Zachos, J. C., and Quattlebaum, T.: A humid climate state during the Paleocene-Eocene thermal maximum, 432, 495–499, 2004.

Bown, T. M. and Kraus, M. J.: Time-stratigraphic reconstruction and integration of paleopedologic, sedimentologic, and biotic events (Willwood Formation, lower Eocene, northwest Wyoming, U.S.A.), 8, 68–80, 1993.

Bown, T. M., Rose, K. D., Simons, E. L., and Wing, S. L.: Distribution and stratigraphic correlation of upper Paleocene and lower Eocene fossil mammal and plant localities of the Fort Union, Willwood, and Tatman Formations, southern Bighorn Basin, Wyoming, 1994.

Cerling, T.: The stable isotopic composition of modern soil carbonate and its relationship to climate, 71, 229–240, 1984.

Cerling, T. E., Hart, J. A., and Hart, T. B.: Stable isotope ecology in the Ituri Forest, 138, 5–12, 2004.

Chen, Z., Ding, Z., Tang, Z., Wang, X., and Yang, S.: Early Eocene carbon isotope excursions: Evidence from the terrestrial coal seam in the Fushun Basin, Northeast China, 41, 3559–3564, https://doi.org/10.1002/2014GL059808, 2014.

Chester, S. G. B., Bloch, J. I., Secord, R., and Boyer, D. M.: A new small-bodied species of Palaeonictis (Creodonta, Oxyaenidae) from the Paleocene-Eocene Thermal Maximum, Journal of Mammalian Evolution, 17, 227–243, https://doi.org/10.1007/s10914-010-9141-y, 2010.

Chew, A. E.: Paleoecology of the early Eocene Willwood mammal fauna from the central Bighorn Basin, Wyoming, Paleobiology, 35, 13–31, https://doi.org/10.1666/07072.1, 2009.

Chew, A. E.: Mammal faunal change in the zone of the Paleogene hyperthermals ETM2 and H2, 11, 1223–1237, https://doi.org/10.5194/cp-11-1223-2015, 2015.

**Deleted:** ¶
Brüggemann, N., Gessler, A., Kayler, Z. E., Keel, S., Badeck, F. Barthel, M., Boeckx, P., Buchmann, N., Brugnoli, E., Esperschütt J., and others: Carbon allocation and carbon isotope fluxes in the plant-soil-atmosphere continuum: a review, 8, 3619–3695, 2011.

**Deleted:** ¶
Cerling, T. E. and Quade, J.: Stable carbon and oxygen isotopes i soil carbonates, edited by: Swart, P. K., Lohmann, K. C., McKen J., and Savin, S., American Geophysical Union, Washington, 217 231 pp., 1993.¶

Chew, A. E. and Oheim, K. B.: Diversity and climate change in the middle-late Wasatchian (early Eocene) Willwood Formation, central Bighorn Basin, Wyoming, Palaeogeography, Palaeoclimatology, Palaeoecology, 369, 67–78, https://doi.org/10.1016/j.palaeo.2012.10.004, 2013.

Clementz, M., Bajpai, S., Ravikant, V., Thewissen, J. G. M., Saravanan, N., Singh, I. B., and Prasad, V.: Early Eocene warming events and the timing of terrestrial faunal exchange between India and Asia, 39, 15–18, 2011.

Clyde, W. C. and Gingerich, P. D.: Mammalian community response to the latest Paleocene thermal maximum: An isotaphonomic study in the northern Bighorn Basin, Wyoming, Geology, 26, 1011–1014, https://doi.org/10.1130/0091-7613(1998)026<1011:MCRTTL>2.3.CO;2, 1998.

Clyde, W. C., Khan, I. H., and Gingerich, P. D.: Stratigraphic response and mammalian dispersal from initial India-Asia collision: Evidence from the Ghazij Formation, Balochistan, Pakistan, 31, 1097–1100, 2003.

Clyde, W. C., Hamzi, W., Finarelli, J. A., Wing, S. L., Schankler, D., and Chew, A.: Basin-wide magnetostratigraphic framework for the Bighorn Basin, Wyoming, 119, 848–859, 2007.

Cojan, I., Moreau, M.-G., and Stott, L. E.: Stable carbon isotope stratigraphy of the Paleogene pedogenic series of southern France as a basis for continental-marine correlation, Geology, 28, 259–262, https://doi.org/10.1130/0091-7613(2000)28<259:SCISOT>2.0.CO;2, 2000.

Coplen, T. B., Brand, W. A., Gehre, M., Gröning, M., Meijer, H. A., Toman, B., and Verkouteren, R. M.: New guidelines for $\delta^{13}C$ measurements, 78, 2439–2441, 2006.

Cramer, B. S., J. D. Wright, D. V. Kent, and M.-P. Aubry: Orbital climate forcing of $\delta^{13}C$ excursions in the late Paleocene–Eocene (chrons C24n –C25n), 18, 1097, 2003.

D'Ambrosia, A. R., Clyde, W. C., Fricke, H. C., Gingerich, P. D., and Abels, H. A.: Repetitive mammalian dwarfing during ancient greenhouse warming events, Sci Adv, 3, https://doi.org/10.1126/sciadv.1601430, 2017.

DeConto, R., Galeotti, S., Pagani, M., Tracy, D., Pollard, D., and Beerling, D.: Hyperthermals and orbitally paced permafrost soil organic carbon dynamics, 2010, PP21E-08, 2010.

**Deleted:** ¶

Codron, J., Codron, D., Lee-Thorp, J. A., Sponheimer, M., Bond J., de Ruiter, D., and Grant, R.: Taxonomic, anatomical, and spat temporal variations in the stable carbon and nitrogen isotopic compositions of plants from an African savanna, Journal of Archaeological Science, 32, 1757–1772, https://doi.org/10.1016/j.jas.2005.06.006, 2005.¶

DeConto, R. M., Galeotti, S., Pagani, M., Tracy, D., Schaefer, K., Zhang, T., Pollard, D., and Beerling, D. J.: Past extreme warming events linked to massive carbon release from thawing permafrost, Nature, 484, 87–91, https://doi.org/10.1038/nature10929, 2012.

Dickens, G. D., Castillo, M. M., and Walker, J. C. G.: A blast of gas in the latest Paleocene: Simulating first-order effects of massive dissociation of oceanic methane hydrate, 25, 259–262, 1997.

Dickens, G. R., O'Neil J. R., Rea, D. K., and Owen, R. M.: Dissociation of oceanic methane hydrate as a cause of the carbon isotope excursion at the end of the Paleocene, 10, 965–971, 1995.

Diefendorf, A. F., Mueller, K. E., Wing, Scott. L., Koch, P. L., and Freeman, K. H.: Global patterns in leaf $^{13}C$ discrimination and implications for studies of past and future climate, Proc Natl Acad Sci USA, 107, 5738, https://doi.org/10.1073/pnas.0910513107, 2010.

Dinarès-Turell, J., Westerhold, T., Pujalte, V., Röhl, U., and Kroon, D.: Astronomical calibration of the Danian stage (Early Paleocene) revisited: Settling chronologies of sedimentary records across the Atlantic and Pacific Oceans, 405, 119–131, https://doi.org/10.1016/j.epsl.2014.08.027, 2014.

D'Onofrio, R., Luciani, V., Fornaciari, E., Giusberti, L., Boscolo Galazzo, F., Dallanave, E., Westerhold, T., Sprovieri, M., and Telch, S.: Environmental perturbations at the early Eocene ETM2, H2, and I1 events as inferred by Tethyan calcareous plankton (Terche section, northeastern Italy), 31, 1225–1247, https://doi.org/10.1002/2016PA002940, 2016.

Ehleringer, J. R.: 11 - Carbon and water relations in desert plants: An isotopic perspective, in: Stable Isotopes and Plant Carbon-water Relations, edited by: Ehleringer, J. R., Hall, A. E., and Farquhar, G. D., Academic Press, San Diego, 155–172, https://doi.org/10.1016/B978-0-08-091801-3.50018-0, 1993.

Foreman, B. Z.: Climate-driven generation of a fluvial sheet sand body at the Paleocene-Eocene boundary in north-west Wyoming (USA), 26, 225–241, https://doi.org/10.1111/bre.12027, 2014.

Foreman, B. Z., Heller, P. L., and Clementz, M. T.: Fluvial response to abrupt global warming at the Palaeocene/Eocene boundary, 491, 92–95, https://doi.org/10.1038/nature11513, 2012.

**Deleted:** ¶

Ehleringer, J. R., Field, C. B., Lin, Z., and Kuo, C.: Leaf carbon isotope and mineral composition in subtropical plants along an irradiance cline, Oecologia, 70, 520–526, https://doi.org/10.1007/BF00379898, 1986.¶
¶
Farquhar, G. D., Ehleringer, J. R., and Hubick, K. T.: Carbon iso discrimination and photosynthesis, Annu. Rev. Plant. Physiol. Pl Mol. Biol., 40, 503–537, https://doi.org/10.1146/annurev.pp.40.060189.002443, 1989.¶

Frieling, J., Svensen, H. H., Planke, S., Cramwinckel, M. J., Selnes, H., and Sluijs, A.: Thermogenic methane release as a cause for the long duration of the PETM, Proc Natl Acad Sci USA, 113, 12059, https://doi.org/10.1073/pnas.1603348113, 2016.

Gibbs, S. J., Bown, P. R., Sessa, J. A., Bralower, T. J., and Wilson, P. A.: Nannoplankton extinction and origination across the Paleocene-Eocene Thermal Maximum, 314, 1770–1773, https://doi.org/10.1126/science.1133902, 2006.

Gingerich, P. D.: Paleocene-Eocene faunal zones and a preliminary analysis of Laramide structural deformation in the Clark's Fork Basin, Wyoming, 185–195, 1983.

Gingerich, P. D.: New earliest Wasatchian mammalian fauna from the Eocene of northwestern Wyoming: Composition and diversity in a rarely sampled high-floodplain assemblage, 28, 1–97, 1989.

Gingerich, P. D.: Mammalian responses to climate change at the Paleocene-Eocene boundary: Polecat Bench record in the northern Bighorn Basin, Wyoming., edited by: Wing, S. L., Gingerich, P. D., Schmitz, B., and Thomas, E., Geological Society of America, Special Paper 369, Boulder, CO, 463–478 pp., 2003.

Gingerich, P. D.: Environment and evolution through the Paleocene–Eocene thermal maximum, 21, 246–253, https://doi.org/10.1016/j.tree.2006.03.006, 2006.

Greenwood, D. R., Moss, P. T., Rowett, A. I., Vadala, A. J., and Keefe, R. L.: Plant communities and climate change in southeastern Australia during the early Paleogene, in: Causes and consequences of globally warm climates in the early Paleogene, Geological Society of America, https://doi.org/10.1130/0-8137-2369-8.365, 2003.

Gutjahr, M., Ridgwell, A., Sexton, P. F., Anagnostou, E., Pearson, P. N., Pälike, H., Norris, R. D., Thomas, E., and Foster, G. L.: Very large release of mostly volcanic carbon during the Palaeocene–Eocene Thermal Maximum, Nature, 548, 573–577, https://doi.org/10.1038/nature23646, 2017.

Higgins, J. A. and Schrag, D. P.: Beyond methane: Towards a theory for the Paleocene–Eocene Thermal Maximum, 245, 523–537, 2006.

Hooker, J. J.: Mammalian faunal change across the Paleocene-Eocene transition in Europe., edited by: Aubry, M.-P. L. S. G. and B. W. A., Columbia University Press, New York, 419–441 pp., 1998.

**Deleted:** ¶
Ghashghaie, J., Badeck, F.-W., Lanigan, G., Nogués, S., Tcherke G., Deléens, E., Cornic, G., and Griffiths, H.: Carbon isotope fractionation during dark respiration and photorespiration in C3 plants, Phytochemistry Reviews, 2, 145–161, https://doi.org/10.1023/B:PHYT.0000004326.00711.ca, 2003.¶

**Deleted:** ¶
Green, G. N. and Drouillard, P. H.: The Digital Geologic Map of Wyoming in ARC/INFO Format: U.S. Geological Survey Open-Report 94-0425, 1994.¶

Jaramillo, C., Ochoa, D., Contreras, L., Pagani, M., Carvajal-Ortiz, H., Pratt, L. M., Krishnan, S., Cardona, A., Romero, M., Quiroz, L., Rodriguez, G., Rueda, M. J., de la Parra, F., Moron, S., Green, W., Bayona, G., Montes, C., Quintero, O., Ramirez, R., Mora, G., Schouten, S., Bermudez, H., Navarrete, R., Parra, F., Alvaran, M., Osorno, J., Crowley, J. L., Valencia, V., and Vervoort, J.: Effects of rapid global warming at the Paleocene-Eocene boundary on neotropical vegetation, Science, 330, 957–961, https://doi.org/10.1126/science.1193833, 2010.

Jennions, S. M., Thomas, E., Schmidt, D. N., Lunt, D., and Ridgwell, A.: Changes in benthic ecosystems and ocean circulation in the Southeast Atlantic across Eocene Thermal Maximum 2, 30, 1059–1077, https://doi.org/10.1002/2015PA002821, 2015.

Katz, M. E., Pak, D. K., Dickens, G. R., and Miller, K. G.: The source and fate of massive carbon input during the latest Paleocene thermal maximum, 286, 1531–1533, 1999.

Kelly, D. C., Bralower, T. J., and Zachos, J. C.: Evolutionary consequences of the latest Paleocene thermal maximum for tropical planktonic Foraminifera, 141, 139–161, 1998.

Kennett, J. P. and Stott, L. D.: Abrupt deep-sea warming, palaeoceanographic changes and benthic extinctions at the end of the Palaeocene, 353, 225–229, 1991.

Koch, P. L., Zachos, J. C., and Gingerich, P. D.: Correlation between isotope records in marine and continental carbon reservoirs near the Palaeocene/Eocene boundary, 358, 319–322, 1992.

Koch, P. L., Zachos, J. C., and Dettman, D. L.: Stable isotope stratigraphy and paleoclimatology of the Paleogene Bighorn Basin (Wyoming, USA), 115, 61–90, 1995.

Koch, P. L., Clyde, W. C., Hepple, R. P., Fogel, M. L., Wing, S. L., and Zachos, J. C.: Carbon and oxygen isotope records from paleosols spanning the Paleocene-Eocene boundary, Bighorn Basin, Wyoming, Geological Society of America Special Papers, 369, 49–64, https://doi.org/10.1130/0-8137-2369-8.49, 2003.

Kohn, M.: Carbon isotope discrimination in C3 land plants is independent of natural variations in $pCO_2$, 2, 35–43, 2016.

Kohn, M. J.: Carbon isotope compositions of terrestrial C3 plants as indicators of (paleo)ecology and (paleo)climate, Proc Natl Acad Sci USA, 107, 19691, https://doi.org/10.1073/pnas.1004933107, 2010.

**Deleted:** ¶
Karberg, N., Pregitzer, K., King, J., Friend, A., and Wood, J.: So carbon dioxide partial pressure and dissolved inorganic carbonat chemistry under elevated carbon dioxide and ozone, 142, 296–30 2005.¶

**Deleted:** ¶
Koch, P. L.: Isotopic reconstruction of past continental environments, 26, 573–613, 1998.¶

Kopf, S., Davidheiser-Kroll, B., and Kocken, I.: Isoreader: An R package to read stable isotope data files for reproducible research, 6, 2878, https://doi.org/10.21105/joss.02878, 2021.

Kraus, M. J.: Alluvial response to differential subsidence: sedimentological analysis aided by remote sensing, Willwood Formation (Eocene), Bighorn Basin, Wyoming, USA, 39, 455–470, 1992.

Kraus, M. J.: Lower Eocene alluvial paleosols: pedogenic development, stratigraphic relationships, and paleosol/landscape associations, 129, 387–406, 1997.

Kraus, M. J., McInerney, F. A., Wing, S. L., Secord, R., Baczynski, A. A., and Bloch, J. I.: Paleohydrologic response to continental warming during the Paleocene-Eocene Thermal Maximum, Bighorn Basin, Wyoming, 370, 196–208, 2013.

Kurtz, A. C., Kump, L. R., Arthur, M. A., Zachos, J. C., and Paytan, A.: Early Cenozoic decoupling of the global carbon and sulfur cycles, 18, https://doi.org/10.1029/2003PA000908, 2003.

Lourens, L. J., Sluijs, A., Kroon, D., Zachos, J. C., Thomas, E., Röhl, U., Bowles, J., and Raffi, I.: Astronomical pacing of late Palaeocene to early Eocene global warming events, 435, 1083–1087, 2005.

Lu, G. and Keller, G.: Planktic foraminiferal faunal turnovers in the subtropical Pacific during the late Paleocene to early Eocene, 25, 97–116, 1995.

McInerney, F. A. and Wing, S. L.: The Paleocene-Eocene Thermal Maximum: A perturbation of carbon cycle, climate, and biosphere with implications for the future, 39, 489–516, 2011.

Moore, E. A. and Kurtz, A. C.: Black carbon in Paleocene–Eocene boundary sediments: A test of biomass combustion as the PETM trigger, 267, 147–152, https://doi.org/10.1016/j.palaeo.2008.06.010, 2008.

Morse, P. E., Chester, S. G. B., Boyer, D. M., Smith, T., Smith, R., Gigase, P., and Bloch, J. I.: New fossils, systematics, and biogeography of the oldest known crown primate Teilhardina from the earliest Eocene of Asia, Europe, and North America, Journal of Human Evolution, 128, 103–131, https://doi.org/10.1016/j.jhevol.2018.08.005, 2019.

Mutterlose, J., Linnert, C., and Norris, R.: Calcareous nannofossils from the Paleocene–Eocene Thermal Maximum of the equatorial Atlantic (ODP Site 1260B): Evidence for tropical warming, 65, 13–31, https://doi.org/10.1016/j.marmicro.2007.05.004, 2007.



**Deleted:** ¶
Lin, G. and Ehleringer, J. R.: Carbon isotopic fractionation does occur during dark respiration in C3 and C4 plants, Plant Physiol. 114, 391, https://doi.org/10.1104/pp.114.1.391, 1997.¶

Parker, S. E. and Jones, R. W.: Isopachous map of Tertiary overburden above latest Cretaceous Lance Formation, Bighorn Basin, Wyoming, Open File Report 86-8, 1986.

R Core Team.: R: A language and environment for statistical computing. R Foundation for Statistical Computing, Vienna, Austria. URL https://www.R-project.org/, 2019

Rose, K. D.: The Clarkforkian land-mammal age and mammalian faunal composition across the Paleocene-Eocene boundary, 26, 1–196, 1981.

Rose, K. D., Chew, A. E., Dunn, R. H., Kraus, M. J., Fricke, H. C., and Zack, S. P.: Earliest Eocene mammalian fauna from the Paleocene-Eocene thermal maximum at sand creek divide, southern Bighorn Basin, Wyoming, 2012.

Samanta, A., Bera, M. K., Ghosh, R., Bera, S., Filley, T., Pande, K., Rathore, S. S., Rai, J., and Sarkar, A.: Do the large carbon isotopic excursions in terrestrial organic matter across Paleocene–Eocene boundary in India indicate intensification of tropical precipitation?, Palaeogeography, Palaeoclimatology, Palaeoecology, 387, 91–103, https://doi.org/10.1016/j.palaeo.2013.07.008, 2013.

Schankler, D. M.: Faunal zonation of the Willwood Formation in the central Bighorn Basin, Wyoming, edited by: Gingerich, P. D., University of Michigan Papers on Paleontology, No. 24, 99–114 pp., 1980.

Schmitz, B. and Pujalte, V.: Abrupt increase in seasonal extreme precipitation at the Paleocene-Eocene boundary, 35, 215–218, 2007.

Schubert, B. A. and Jahren, A. H.: Reconciliation of marine and terrestrial carbon isotope excursions based on changing atmospheric $CO_2$ levels, Nature Communications, 4, 1653, https://doi.org/10.1038/ncomms2659, 2013.

Secord, R., Wing, S. L., and Chew, A.: Stable isotopes in early Eocene mammals as indicators of forest canopy structure and resource partitioning, 34, 282–300, 2008.

Secord, R., Bloch, J. I., Chester, S. G. B., Boyer, D. M., Wood, A. R., Wing, S. L., Kraus, M. J., McInerney, F. A., and Krigbaum, J.: Evolution of the Earliest Horses Driven by Climate Change in the Paleocene-Eocene Thermal Maximum, 335, 959–962, https://doi.org/10.1126/science.1213859, 2012.

**Deleted:** ¶
O'Leary, M. H.: Carbon Isotopes in Photosynthesis, BioScience, 328–336, https://doi.org/10.2307/1310735, 1988.¶

**Deleted:** ¶
Schubert, B. A. and Jahren, A. H.: The effect of atmospheric CO concentration on carbon isotope fractionation in C3 land plants, 29–43, 2012.¶

Smith, F. A., Wing, S. L., and Freeman, K. H.: Magnitude of the carbon isotope excursion at the Paleocene-Eocene thermal maximum: the role of plant community change, 262, 50–65, 2007.

Smith, T., Rose, K. D., and Gingerich, P. D.: Rapid Asia–Europe–North America geographic dispersal of earliest Eocene primate *Teilhardina* during the Paleocene–Eocene Thermal Maximum, 103, 11223–11227, 2006.

Snell, K. E., Thrasher, B. L., Eiler, J. M., Koch, P. L., Sloan, L. C., and Tabor, N. J.: Hot summers in the Bighorn Basin during the early Paleogene, 41, 55–58, https://doi.org/10.1130/G33567.1, 2013.

Speijer, R., Scheibner, C., Stassen, P., and Morsi, A.-M. M.: Response of marine ecosystems to deep-time global warming: a synthesis of biotic patterns across the Paleocene-Eocene Thermal Maximum (PETM), 105, 6–16, 2012.

Stap, L., Sluijs, A., Thomas, E., and Lourens, L.: Patterns and magnitude of deep-sea carbonate dissolution during Eocene Thermal Maximum 2 and H2, Walvis Ridge, southeastern Atlantic Ocean, 24, PA1211: 10.1029/2008PA001655, 2009.

Stap, L., Lourens, L. J., Thomas, E., Sluijs, A., Bohaty, S., and Zachos, J. C.: High-resolution deep-sea carbon and oxygen isotope records of Eocene Thermal Maximum 2 and H2, 38, 607–610, 2010.

Stewart, G., Turnbull, M., Schmidt, S., and Erskine, P.: $^{13}C$ natural abundance in plant communities along a rainfall gradient: a biological integrator of water availability, Functional Plant Biol., 22, 51–55, 1995.

Strait, S.: New Wa-0 mammalian fauna from Castle Gardens in the southeastern Bighorn Basin, 33, 127–143, 2001.

Svensen, H., Planke, S., Malthe-Sorenssen, A., Jamtveit, B., Myklebust, R., Eidem, T. R., and Rey, S. S.: Release of methane from a volcanic basin as a mechanism for initial Eocene global warming, 429, 542–545, 2004.

Tauxe, L., Gee, J., Gallet, Y., Pick, T., and Bown, T.: Magnetostratigraphy of the Willwood Formation, Bighorn Basin, Wyoming: new constraints on the location of Paleocene/Eocene boundary, Earth and Planetary Science Letters, 125, 159–172, https://doi.org/10.1016/0012-821X(94)90213-5, 1994.

Thomas, E.: Biogeography of the late Paleocene benthic foraminiferal extinction, 214–243, 1998.

Thomas, E.: Cenozoic mass extinctions in the deep sea: What perturbs the largest habitat on Earth?, 424, 1, 2007.

Thomas, E. and Shackleton, N. J.: The Paleocene-Eocene benthic foraminiferal extinction and stable isotope anomalies, edited by: Knox, R. W. O., Corfield, R. M., and Dunay, R. E., Geological Society [London] Special Publication 101, London, 401–441 pp., 1996.

Thomas, E., Zachos, J. C., and Bralower, T. J.: Deep-sea environments on a warm Earth: latest Paleocene-early Eocene, in: Warm Climates in Earth History, edited by: Huber, B. T., Macleod, K. G., and Wing, S. L., Cambridge University Press, 132–160, https://doi.org/10.1017/CBO9780511564512.006, 2000.

Westerhold, T., Röhl, U., Donner, B., and Zachos, J. C.: Global extent of early Eocene hyperthermal events: A new Pacific benthic foraminiferal isotope record from Shatsky Rise (ODP Site 1209), Paleoceanography and Paleoclimatology, 33, 626–642, https://doi.org/10.1029/2017PA003306, 2018.

Westerhold, T., Marwan, N., Drury, A. J., Liebrand, D., Agnini, C., Anagnostou, E., Barnet, J. S. K., Bohaty, S. M., De Vleeschouwer, D., Florindo, F., Frederichs, T., Hodell, D. A., Holbourn, A. E., Kroon, D., Lauretano, V., Littler, K., Lourens, L. J., Lyle, M., Pälike, H., Röhl, U., Tian, J., Wilkens, R. H., Wilson, P. A., and Zachos, J. C.: An astronomically dated record of Earth's climate and its predictability over the last 66 million years, Science, 369, 1383, https://doi.org/10.1126/science.aba6853, 2020.

Wickham et al.: Welcome to the tidyverse. Journal of Open Source Software, 4(43), 1686, https://doi.org/10.21105/joss.01686, 2019

Wing, S. L., Harrington, G. J., Smith, F. A., Bloch, J. I., Boyer, D. M., and Freeman, K. H.: Transient floral change and rapid global warming at the Paleocene-Eocene boundary, 310, 993–996, 2005.

Woodburne, M. O., Gunnell, G. F., and Stucky, R. K.: Climate directly influences Eocene mammal faunal dynamics in North America, Proceedings of the National Academy of Sciences, 106, 13399–13403, https://doi.org/10.1073/pnas.0906802106, 2009.

Zachos, J. C., Pagani, M., Sloan, L., Thomas, E., and and Billups, K.: Trends, rythyms, and aberrations in global climate 65 Ma to Present, 292, 686–693, 2001.

Zachos, J. C., Röhl, U., Schellenberg, S. A., Sluijs, A., Hodell, D. A., Kelly, D. C., Thomas, E., Nicolo, M., Raffi, I., Lourens, L. J., McCarren, H., and Kroon, D.: Rapid acidification of the ocean during the Paleocene-Eocene Thermal Maximum, 308, 1611–1615, 2005.

**Deleted:** ¶
Van der Merwe, N. J. and Medina, E.: The canopy effect, carbon isotope ratios and foodwebs in Amazonia, Journal of Archaeolog Science, 18, 249–259, https://doi.org/10.1016/0305-4403(91)900 V, 1991.¶

**Deleted:** ¶
Wynn, J. G.: Carbon isotope fractionation during decomposition organic matter in soils and paleosols: Implications for paleoecological interpretations of paleosols, 251, 437–448, https://doi.org/10.1016/j.palaeo.2007.04.009, 2007.¶
¶
Wynn, J. G., Bird, M. I., and Wong, V. N. L.: Rayleigh distillatio and the depth profile of $^{13}C/^{12}C$ ratios of soil organic carbon from soils of disparate texture in Iron Range National Park, Far North Queensland, Australia, Geochimica et Cosmochimica Acta, 69, 1961–1973, https://doi.org/10.1016/j.gca.2004.09.003, 2005.¶

Zachos, J. C., Dickens, G. R., and Zeebe, R. E.: An early Cenozoic perspective on greenhouse warming and carbon-cycle dynamics, 451, 279–283, 2008.

Zachos, J. C., McCarren, H., Murphy, B., Röhl, U., and Westerhold, T.: Tempo and scale of late Paleocene and early Eocene carbon isotope cycles: Implications for the origin of hyperthermals, 299, 242–249, https://doi.org/10.1016/j.epsl.2010.09.004, 2010.

**Deleted:** ¶
Zamanian, K., Pustovoytov, K., and Kuzyakov, Y.: Pedogenic carbonates: Forms and formation processes, Earth-Science Revie 157, 1–17, https://doi.org/10.1016/j.earscirev.2016.03.003, 2016